Speeding-up Symbol-Level Precoding Using Separable and Dual Optimizations

Junwen Yang, *Graduate Student Member, IEEE,* Ang Li, *Senior Member, IEEE,* Xuewen Liao, *Member, IEEE,* and Christos Masouros, *Senior Member, IEEE*

***Abstract*—Symbol-level precoding (SLP) can fully exploit the multi-user interference in the downlink. This paper investigates fast SLP algorithms for phase-shift keying (PSK) and quadrature amplitude modulation (QAM). In particular, we prove that the weighted max-min signal-to-interference-plus-noise ratio (SINR) balancing (SB) SLP problem with PSK signaling is not separable, which is contrary to the power minimization (PM) SLP problem, and accordingly, existing decomposition methods are not applicable. To tackle this issue, we establish an explicit duality between the SB-SLP and PM-SLP problems with PSK modulation. The proposed duality enables simultaneously obtaining the solutions to the SB-SLP and PM-SLP problems. We concurrently propose a closed-form power scaling algorithm to address the SB-SLP problem by the solution to the PM-SLP problem, via which the separability can be leveraged to decompose the problem. In terms of QAM signaling, a succinct model is used to formulate the PM-SLP problem and convert it into a separable equivalent. The new problem is decomposed into several simple parallel subproblems with closed-form solutions, employing the proximal Jacobian alternating direction method of multipliers (PJ-ADMM). We further prove that the proposed duality can be generalized to the multi-level modulation case, based on which a power scaling parallel inverse-free algorithm is proposed to solve the SB-SLP problem with QAM signaling. Numerical results show that the proposed algorithms offer optimal performance with lower complexity than the state-of-the-art.**

***Index Terms*—MU-MISO, symbol-level precoding, separability, duality, inverse problem, ADMM.**

Manuscript received February 23, 2023; revised July 3, 2023; accepted August 15, 2023. The work of Ang Li was supported in part by the Young Elite Scientists Sponsorship Program by CIC under Grant 2021QNRC001, in part by the National Natural Science Foundation of China under Grant 62101422, and in part by the Science and Technology Program of Shaanxi Province under Grant 2021KWZ-01. The work of Xuewen Liao was supported in part by the National Key Research and Development Project of China under Grant 2019YFB2101600, in part by the Science and Technology Program of Shaanxi Province under Grant 2021GXLH-Z-038, and in part by the Open Research Fund of the National Mobile Communications Research Laboratory, Southeast University, under Grant 2020D12. The work of Christos Masouros was supported by the Engineering and Physical Sciences Research Council EPSRC project LeanCom EP/S028455/1. Part of this work was presented at the IEEE Vehicular Technology Conference (VTC2023-Spring), Florence, Italy, June 2023 [1]. The associate editor coordinating the review of this manuscript and approving it for publication was Prof. G. Kaddoum. *(Corresponding authors: Xuewen Liao; Ang Li.)*

Junwen Yang and Ang Li are with the School of Information and Communications Engineering, Faculty of Electronic and Information Engineering, Xi'an Jiaotong University, Xi'an, Shaanxi 710049, China (e-mail: jwyang@stu.xjtu.edu.cn; ang.li.2020@xjtu.edu.cn).

Xuewen Liao is with the School of Information and Communications Engineering, Faculty of Electronic and Information Engineering, Xi'an Jiaotong University, Xi'an, Shaanxi 710049, China, and also with the National Mobile Communications Research Laboratory, Southeast University, Nanjing 210096, China (e-mail: yeplos@mail.xjtu.edu.cn).

Christos Masouros is with the Department of Electronic and Electrical Engineering, University College London, London WC1E 7JE, U.K. (e-mail: c.masouros@ucl.ac.uk).

I. Introduction

INTERFERENCE is one of the major nuisances that deteriorate the performance of wireless communication systems [2]. To achieve a promising performance for multi-user transmission in the downlink, precoding has been recognized as an indispensable interference management technique at the transmitter side [3]. Conventional precoders in multi-antenna systems aim to suppress, mitigate, or eliminate interference because it distorts the desired signal just like noise. For instance, high-performance nonlinear precoders such as dirty paper precoding (DPC) [4] and Tomlinson-Harashima precoding (THP) [5], [6] compensate for signal distortion caused by interference through pre-subtracting it successively. As a result, the precoded signal becomes a nonlinear transformation of the data symbols. The vector perturbation (VP) precoding combines the regularization of channel inversion and the perturbation of transmit symbols [7]. It jointly considers all the transmit symbols to generate an integer perturbation vector for data symbols using a sphere encoder, which differs from the DPC and THP that successively cancel the interference. Contrary to the nonlinear one, block-level precoding (BLP) generally uses only the channel state information (CSI) to calculate the precoding matrix, which is independent of the transmit data symbols. Zero-forcing (ZF) precoding is one of the typical linear precoders, which eliminates the multi-user interference via the inverse of the channel matrix [8]. Such a simple operation will however augment the noise, thus limiting the performance. To this end, regularized ZF (RZF) precoding suppresses interference by introducing regularization to channel inversion [9].

In addition to the above closed-form precoding, object-oriented linear precoding is another line of work, which designs the precoder involving specific quality of service (QoS) metrics and transmit power budgets. As it is generally modeled as a constrained optimization problem, also known as optimization-based precoding, e.g., the signal-to-interference-plus-noise ratio (SINR)-constrained power minimization (PM) precoding [10], the power-constrained max-min SINR balancing (SB) precoding [11]–[13], and the power-constrained weighted sum-rate (WSR) maximization precoding [14]. Early works focus on designing linear or block-level precoders through optimization, assuming independent and identically distributed (i.i.d.) data symbols. It has been revealed that the PM and SB problems are inverse problems [13]. Based on this inversion property, the SB problem can be solved by iteratively solving the PM problem for different SINR constraints along

with a one-dimension bisection search [13].

Only CSI is employed in the above closed-form linear precoding and optimization-based linear precoding. Nevertheless, information on the data symbols, which is also available at the transmitter, is not exploited for conventional BLP. They ignore that once interference can be controlled instantaneously, it may be beneficial to signal detection [15]. Therefore, instead of avoiding interference by leveraging the aforementioned conventional precoding schemes, recent works have proposed to exploit the known interference as a useful signal power based on the concept of constructive interference (CI) [15]. Since data symbols vary among symbol slots, CI precoding is usually designed on a symbol-by-symbol basis, which is known as symbol-level precoding (SLP) [16]–[20]. A seminal treatment of CI precoding was first proposed in a closed-form nonlinear precoding [21]. The concept has been extended to optimization-based nonlinear precoding, attracting more and more attention because of its superior performance to its linear counterpart [15]–[17].

The objective-oriented CI precoding concerning PM-SLP and SB-SLP problems was first proposed in [16], where all interference is strictly aligned with the data symbols, which followed the principle in [22]. Improvement has been made in [15] by designing a more relaxed optimization for received symbols based on the proposed CI region. The above optimization-based CI-SLP works focus on only phase-shift keying (PSK) signaling. CI in quadrature amplitude modulation (QAM) constellation was first discussed in [23], and the first optimization-based CI-SLP concerning the PM problem with square multi-level modulation is studied in [24]. The SB-SLP problem with multi-level modulation (or generic two-dimensional constellations) was investigated in [25].

Recent years have witnessed extensive endeavors to address low-complexity CI-SLP solutions. These include the efficient gradient projection algorithm (EGPA) to solve the Lagrangian dual problem of PM-SLP [15], closed-form suboptimal solutions for PM-SLP [26], [27], derivations of the optimal precoding structure for SB-SLP with iterative algorithms [28], [29], the CI-based BLP (CI-BLP) approach [30], and the grouped SLP (G-SLP) approach [31]. Unfortunately, none of the above works have investigated the separable structure of SLP problems. They all focus on centralized algorithms instead of parallel and distributed solutions. More recently, the separability of the PM-SLP problem with PSK signaling has been revealed in [32], where parallel algorithms based on the alternating direction method of multipliers (ADMM) have been further proposed to solve the PM-SLP problem by exploiting its separable structure. However, there are remaining limitations of existing works to be overcome. Specifically, the SB-SLP problem with PSK signaling still needs to be addressed, and whether it is separable is not yet clear. In addition, the existence or absence of separability in PM-SLP and SB-SLP problems with multi-level modulation remains unestablished. Moreover, there is still a need to explore the parallel algorithms for multi-level modulation.

Motivated by the above observations, in this paper we address the SB-SLP problem with PSK signaling as well as the PM/SB-SLP problems with multi-level modulation. For clarity, the main contributions of this paper are summarized as follows:

1) *Separability Analysis for SLP:* We first investigate the SB-SLP problem with PSK signaling. By rearranging the canonical problem formulation, we prove that this problem is not separable, hence it is not possible to decompose it into parallel subproblems. We capture and present the key difference between the two considered problems, i.e., the presence and absence of separability. This is in sharp contrast with existing literature [15]–[18].
2) *Explicit Duality and Power Scaling Algorithm for SLP:* More importantly, we establish an explicit duality between the PM-SLP and SB-SLP problems with PSK signaling, which facilitates solving a pair of PM-SLP and SB-SLP problems simultaneously. This is a novel one-to-one mapping between the two problems, different from the existing inverse relation in [16]. A one-step power scaling algorithm that solves the SB-SLP problem using the solution to the PM-SLP problem is developed, via which the parallel algorithms based on the separability are applicable to the SB-SLP problem. Moreover, the proposed explicit duality for SLP is not confined to the proposed separability analysis. It can be generalized to any algorithm solving the PM-SLP problem, such that the inseparable SB-SLP problem can be solved by the solution to the PM-SLP problem.
3) *Parallel Inverse-Free Solution to PM-SLP Problem with Multi-Level Modulation:* We then tackle the PM-SLP problem with multi-level modulation, for which the separability is analyzed. This problem is formulated as a nonlinear programming problem with equality and inequality CI constraints. Although separability is proven to exist for the PM-SLP problem with multi-level modulation, the parallel inverse-free SLP algorithms for PSK signaling are not directly feasible due to the inner constellation points. To obtain a low-complexity algorithm taking advantage of the separability, we introduce a slack variable converting the inequality CI constraints into equality. The feasible region of the slack variable is a polyhedral related to data symbols, which differs from the PM-SLP problem with PSK signaling considered in [32]. The proximal Jacobian alternating direction method of multipliers (PJ-ADMM) is leveraged to solve the reformulated problem, arriving at a modified parallel inverse-free SLP (PIF-SLP) algorithm.
4) *Power Scaling Parallel Inverse-Free Solution to SB-SLP Problem with Multi-Level Modulation:* The SB-SLP problem with multi-level modulation is studied. Similar to the PSK signaling case, we prove that this problem is not separable. The explicit duality of the two considered problems with multi-level modulation is further proven, therefore the proposed power scaling algorithm can be applied to multi-level modulation. Based on the modified PIF-SLP algorithm and the power scaling algorithm, a power scaling PIF-SLP (SPIF-SLP) algorithm is proposed to solve the SB-SLP problem with

multi-level modulation.

Simulation results are conducted to validate our analysis of the separability and duality. They also demonstrate that the proposed parallelizable algorithms can greatly reduce the computational complexity of CI-SLP without sacrificing performance compared to existing works. Specifically, the most significant execution time reduction can be observed in the PM-SLP problem with multi-level modulation. Our algorithm is also shown to be competent for the SB-SLP problem for the challenging fully-loaded systems with multi-level modulation, although it requires more iterations than other scenarios.

The main novelty of this paper with respect to our previous work [32] is the parallelizable methodology on the inseparable SB-SLP problem. Although the separability of the PM-SLP problem with PSK modulation has been considered in [32] for the first time in the literature, and parallelizable algorithms have been therein proposed to reduce the complexity, the analysis and algorithms cannot directly be extended to the SB-SLP problems. This is because the PM-SLP and SB-SLP problems have different mathematical formulations and underlying rationales [15]–[17]. To address this challenge, the methodology proposed herein resorts to dual and separable optimizations. We rigorously prove an explicit duality between the PM-SLP and weighted SB-SLP problems, which is used to solve the inseparable SB-SLP problem by the parallelizable method.

The remainder of this paper is organized as follows. Section II introduces the system model and CI, as well as the canonical PM-SLP and SB-SLP problems with PSK signaling. Section III reformulates the two canonical problems in PSK modulation, establishes the proposed explicit duality between them, and further develops a closed-form power scaling algorithm for the SB-SLP problem. Section IV addresses the PM-SLP and SB-SLP problems with QAM modulation, where we propose our PIF-SLP algorithm for the former and the SPIF-SLP algorithm for the latter. The explicit duality is also generalized to the QAM case. Section V provides the computational complexity analysis. Numerical results are presented in Section VI, and Section VII concludes the paper.

Notation: $(\cdot)^T$, $(\cdot)^H$, and $(\cdot)^{-1}$ denote transpose, conjugate transpose, and inverse operators, respectively. $\mathbb{C}^{M\times N}$ and $\mathbb{R}^{M\times N}$ denote the sets of $M \times N$ matrices with complex-valued and real-valued entries, respectively. $|\cdot|$ represents the absolute value of a real-valued scalar or the modulus of a complex-valued scalar. $\|\cdot\|$ denotes the Euclidean norm of a vector or spectral norm of a matrix. $\|\cdot\|_\infty$ represents the ℓ_∞-norm of a vector. $\Re\{\cdot\}$ and $\Im\{\cdot\}$ respectively denote the real part and imaginary part of a complex-valued input. $\succeq$ and $\trianglerighteq$ denote the element-wise inequality and generalized inequality, respectively. $\mathbf{0}$, $\mathbf{1}$, and $\mathbf{I}$ represent respectively, the all-zeros vector, the all-ones vector, and the identity matrix with appropriate dimensions. $\oslash$ denotes the element-wise division. $diag\{\cdot\}$ returns a vector consisting of the main diagonal elements of a input matrix.

II. System Model and Problem Formulation

This section presents the system model and briefly reviews the concept of CI in the context of PSK signaling, followed by the PM-SLP and SB-SLP problem formulation with PSK modulation.

A. System Model

We consider a downlink multi-user multiple-input single-output (MU-MISO) system, where a base station (BS) equipped with N_t antennas provides service for K single-antenna users in the same time-frequency resource. The independent random data bits for each user are modulated to normalized data symbols. The data symbol vector $\tilde{\mathbf{s}} \triangleq [\tilde{s}_1, \cdots, \tilde{s}_K]^T \in \mathbb{C}^K$ contains the overall K data symbols in a symbol slot, which is mapped to the transmit signal $\tilde{\mathbf{x}} \triangleq [\tilde{x}_1, \cdots, \tilde{x}_{N_t}]^T \in \mathbb{C}^{N_t}$ at the BS via SLP. The received signal of user k in one symbol slot is expressed as

$$\tilde{y}_k = \tilde{\mathbf{h}}_k^T \tilde{\mathbf{G}} \tilde{\mathbf{s}} + \tilde{z}_k = \tilde{\mathbf{h}}_k^T \sum_{i=1}^{K} \tilde{\mathbf{g}}_i \tilde{s}_i + \tilde{z}_k = \tilde{\mathbf{h}}_k^T \tilde{\mathbf{x}} + \tilde{z}_k, \quad (1)$$

where $\tilde{\mathbf{h}}_k \in \mathbb{C}^{N_t}$ denotes the quasi-static Rayleigh flat-fading channel vector between BS and user k, $\tilde{\mathbf{g}}_i \in \mathbb{C}^{N_t}$ represents the i-th column of $\tilde{\mathbf{G}}$, i.e., the precoder for $\tilde{s}_i$, and $\tilde{z}_k \sim \mathcal{CN}(0, \sigma_k^2)$ is the complex-valued additive white Gaussian noise at user k. The channel matrix is denoted by $\tilde{\mathbf{H}} \triangleq [\tilde{\mathbf{h}}_1, \cdots, \tilde{\mathbf{h}}_K]^T \in \mathbb{C}^{K\times N_t}$. To focus on the precoding design, perfect CSI is assumed.

It should be noted that the dimension of the precoding matrix $\tilde{\mathbf{G}}$ is K times as the transmit signal $\tilde{\mathbf{x}}$ in the complex domain. This observation motivates us to choose the transmit signal $\tilde{\mathbf{x}}$ rather than the precoding matrix $\tilde{\mathbf{G}}$ as the variable to be optimized to reduce the problem dimension/complexity. For the single-level modulation with unit-amplitude constellation points, once the optimal transmit signal $\tilde{\mathbf{x}}$ is obtained, the optimal precoding matrix $\tilde{\mathbf{G}}$ can be recovered by the virtual physical-layer multicasting relation for SLP proposed in [15], [16]:

$$\tilde{\mathbf{g}}_1 = \frac{\tilde{\mathbf{x}}}{K}, \tilde{\mathbf{g}}_k = \frac{\tilde{\mathbf{x}}\tilde{s}_1}{K\tilde{s}_k}, \forall k \neq 1. \quad (2)$$

As (2) cannot be generalized to multi-level modulation, we propose to compute the precoding matrix $\tilde{\mathbf{G}}$ by the following versatile formulation that can be employed for arbitrary modulations:

$$\tilde{\mathbf{G}} = \tilde{\mathbf{x}} \frac{\tilde{\mathbf{s}}^H}{\tilde{\mathbf{s}}^H \tilde{\mathbf{s}}}. \quad (3)$$

The above approach that recovers the precoding matrix from the transmit signal not only enjoys a much lower problem dimension which demands less computation complexity compared to conventional SLP that naively optimizes the precoding matrix, but also provides compatibility with conventional baseband and radio-frequency systems dedicated to constructing linear precoders.

SLP can coherently transmit the data symbol of one user using multiple transmit antennas, which leads to beamforming gain and array gain. In practical systems adopting multi-level modulation, user k need to rescale the received signal $\tilde{y}_k$ by a factor $\phi \in \mathbb{R}$ broadcasted by the BS to compute the estimated symbol of the transmitted data symbol $\tilde{s}_k$. The estimated symbol of user k is given by $\hat{s}_k \triangleq \phi \tilde{y}_k$.

This article has been accepted for publication in IEEE Transactions on Communications. This is the author's version which has not been fully edited and content may change prior to final publication. Citation information: DOI 10.1109/TCOMM.2023.3308149

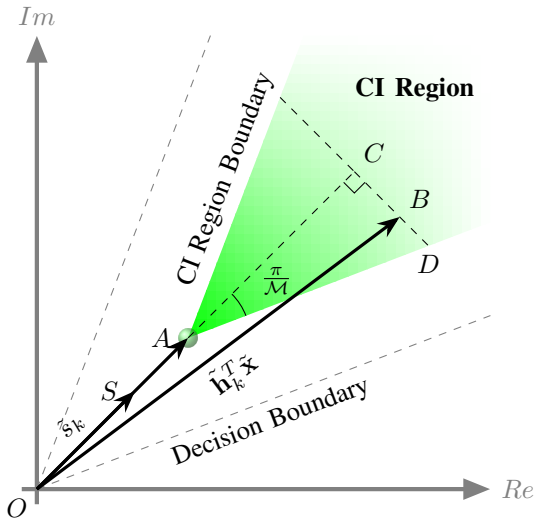

Fig. 1. Illustration of CI regions for a generic $\mathcal{M}$-PSK constellation.

B. Constructive Interference

To predict and further exploit the interference, CI precoding optimizes the transmit signal by judiciously utilizing CSI and data symbols, such that all the multi-user interference can add up constructively at each receiver side [17]. As a consequence, the received instantaneous SINR at user k is given by

$$\mathrm{SINR}_k \triangleq \frac{|\tilde{\mathbf{h}}_k^T\tilde{\mathbf{x}}|^2}{\sigma_k^2}. \tag{4}$$

Since all interference is exploited via CI precoding, the instantaneous SINR is equivalent to the conventional signal-to-noise ratio (SNR).

The optimization-based CI precoding attains CI leveraging the CI constraints. For the sake of illustration, the geometric interpretation of CI is shown in Fig. 1. Without loss of generality, denote the symbol of interest of user k by $\tilde{s}_k$, which is an arbitrary constellation point drawn from a normalized $\mathcal{M}$-PSK constellation, corresponding to $\overrightarrow{OS}$. The received noiseless signal of user k can be expressed as $\tilde{\mathbf{h}}_k^T\tilde{\mathbf{x}}$, which is denoted by $\overrightarrow{OB}$ in Fig. 1. For a given instantaneous SINR threshold γ_k for user k, the nominal constellation point is equivalent to $\sqrt{\gamma_k}\sigma_k\tilde{s}_k$. We introduce $\overrightarrow{OA} = \sqrt{\gamma_k}\sigma_k\tilde{s}_k$ as the nominal constellation point, which is also the only vertex of the associated CI region, where the CI region refers to a polyhedron bounded by hyperplanes parallel to decision boundaries or Voronoi edges of the constellation [15], [33]. The CI region associated with the nominal constellation point $\overrightarrow{OA}$ is depicted as the green-shaded area in Fig. 1. When $\overrightarrow{OB}$ is located in the depicted CI region, then the received signal is pushed away from decision boundaries, thus further into the correct decision region. In the meantime, the instantaneous SINR is guaranteed to be no less than $\gamma_k\left|\tilde{s}_k\right|^2$. Geometrically, if $\overrightarrow{OB}$ is orthogonally decomposed along $\overrightarrow{OS}$, then we have $\overrightarrow{OB} = \overrightarrow{OC} + \overrightarrow{CB}$, where $\overrightarrow{OC} \perp \overrightarrow{CB}$. The component of $\overrightarrow{OB}$ along $\overrightarrow{OS}$ is $\overrightarrow{OC}$, with $\left|\overrightarrow{OC}\right| = \Re\left\{\frac{|\tilde{s}_k|}{\tilde{s}_k}\tilde{\mathbf{h}}_k^T\tilde{\mathbf{x}}\right\}$. Consequently, one of the criteria that specifies the location of $\overrightarrow{OB}$ in the CI region is $\left|\overrightarrow{CD}\right| \geq \left|\overrightarrow{CB}\right|$, where D denotes the intersection of $\overrightarrow{CB}$ and its nearest CI region boundary. The corresponding explicit mathematical formulation of CI constraints for $\mathcal{M}$-PSK signaling can be written as $\Re\{\hat{\mathbf{h}}_k^T\tilde{\mathbf{x}}\} - \frac{|\Im\{\hat{\mathbf{h}}_k^T\tilde{\mathbf{x}}\}|}{\tan\frac{\pi}{\mathcal{M}}} \geq \sqrt{\gamma_k}\sigma_k,\ \forall k$, where $\hat{\mathbf{h}}_k^T \triangleq \frac{\tilde{\mathbf{h}}_k^T}{\tilde{s}_k}$, γ_k denotes the pre-defined instantaneous SINR threshold for user k. It is worth noting that the SINR constraint for each user is already incorporated in the CI constraint.

C. Problem Formulation

1) PM-SLP Problem: The PM-SLP problem aims to minimize the total transmit power subject to CI constraints. This optimization problem has the following mathematical form [15]:

$$\begin{aligned}\min_{\tilde{\mathbf{x}}} \quad & \|\tilde{\mathbf{x}}\|^2 \\ \text{s.t. } & \Re\{\hat{\mathbf{h}}_k^T\tilde{\mathbf{x}}\} - \frac{|\Im\{\hat{\mathbf{h}}_k^T\tilde{\mathbf{x}}\}|}{\tan\frac{\pi}{\mathcal{M}}} \geq \sqrt{\gamma_k}\sigma_k,\ \forall k.\end{aligned} \tag{5}$$

The above problem is linearly constrained quadratic programming. It is accordingly convex and can be solved via off-the-shelf solvers. But most standard solvers, e.g., SeDuMi and SDPT3, are based on the high-complexity interior-point method (IPM). To alleviate the computational burden, recently a number of algorithms were proposed, e.g., the EGPA [15], suboptimal closed-form solution [26], and improved suboptimal closed-form solution [27].

More recently, we revealed the separability of the PM-SLP problem with PSK modulation and proposed a parallelizable and inversion-free CI-SLP precoding approach in our previous work [32] based on the PJ-ADMM framework, which includes the PIF-SLP algorithm. More details please refer to [32] and the references therein.

2) SB-SLP Problem: As mentioned in Section I, another typical SLP is the SB-SLP problem, which focuses on fairness in the system by maximizing the minimum instantaneous SINR over all users subject to a total transmit power constraint. This problem is formulated as (6) on the top of the next page, where p denotes the total transmit power budget, and, with a little abuse of notation, $\frac{1}{\sqrt{\gamma_k}}$ denotes the square root of the weight of SINR_k in the context of the SB-SLP problem.

The original (weighted) max-min SB-SLP problem can be equivalently converted to a more tractable standard second-order cone programming (SOCP) problem [15], given by

$$\begin{aligned}\max_{\tilde{\mathbf{x}},\mu} \quad & \mu \\ \text{s.t. } & \Re\{\hat{\mathbf{h}}_k^T\tilde{\mathbf{x}}\} - \frac{|\Im\{\hat{\mathbf{h}}_k^T\tilde{\mathbf{x}}\}|}{\tan\frac{\pi}{\mathcal{M}}} \geq \mu\sqrt{\gamma_k}\sigma_k,\ \forall k, \\ & \|\tilde{\mathbf{x}}\|^2 \leq p.\end{aligned} \tag{7}$$

Similar to the PM-SLP problem, the problem above can be solved using standard solvers for convex optimization. To solve it more efficiently, the derivation of the optimal structure is used to obtain its Lagrangian dual problem, which is shown to be quadratic over a simplex [28]. Based on the solution structure analysis, an iterative closed-form scheme was proposed in [28] for PSK signaling.

$$\max_{\tilde{\mathbf{x}}} \min_{k} \min \left\{ \frac{1}{\sqrt{\gamma_k}\sigma_k} \left(\Re\{\hat{\mathbf{h}}_k^T \tilde{\mathbf{x}}\} - \frac{\Im\{\hat{\mathbf{h}}_k^T \tilde{\mathbf{x}}\}}{\tan\frac{\pi}{\mathcal{M}}} \right), \frac{1}{\sqrt{\gamma_k}\sigma_k} \left(\Re\{\hat{\mathbf{h}}_k^T \tilde{\mathbf{x}}\} + \frac{\Im\{\hat{\mathbf{h}}_k^T \tilde{\mathbf{x}}\}}{\tan\frac{\pi}{\mathcal{M}}} \right) \right\} \quad \text{s.t. } \|\tilde{\mathbf{x}}\|^2 \le p \tag{6}$$

It is then natural to ask whether the SB-SLP problem is separable or not because this is essential for the employment of the PIF-SLP algorithm. To answer this question, Section III shows that separability does not exist in the SB-SLP problem with PSK modulation. By deriving an explicit duality between the two problems, Section III further proposes a closed-form one-step power scaling algorithm to solve the SB-SLP problem, provided that the solution to the PM-SLP problem is given.

III. Proposed Closed-Form Power Scaling Algorithm for SB-SLP

This section reformulates the SB-SLP and PM-SLP problems with PSK modulation, then derives the one-to-one mapping between a pair of PM-SLP and SB-SLP problems with PSK modulation. Based on this, a closed-form power scaling algorithm is proposed to solve the SB-SLP problem. Accordingly, the separable structure of the PM-SLP problem with PSK modulation can be employed in solving both the PM-SLP and SB-SLP problems.

A. Problem Reformulation

For notation simplicity, we adopt the equivalent real-valued notations. By using the complex-to-real transformation, the real-valued equivalent of (7) can be written as

$$\begin{aligned} \max_{\mathbf{x},\mu} \quad & \mu \\ \text{s.t. } & \mathbf{T}\mathbf{S}_k\mathbf{H}_k\mathbf{x} \succeq \mu\sqrt{\gamma_k}\sigma_k\mathbf{1},\ \forall k, \\ & \|\mathbf{x}\|^2 \le p, \end{aligned} \tag{8}$$

where $\mathbf{x} \triangleq \begin{bmatrix} \Re\{\tilde{\mathbf{x}}\} \\ \Im\{\tilde{\mathbf{x}}\} \end{bmatrix} \in \mathbb{R}^{2N_t}$, $\mathbf{T} \triangleq \begin{bmatrix} 1 & -\frac{1}{\tan\frac{\pi}{\mathcal{M}}} \\ 1 & \frac{1}{\tan\frac{\pi}{\mathcal{M}}} \end{bmatrix} \in \mathbb{R}^{2\times 2}$, $\mathbf{S}_k \triangleq \begin{bmatrix} \Re\left\{\frac{1}{\tilde{s}_k}\right\} & -\Im\left\{\frac{1}{\tilde{s}_k}\right\} \\ \Im\left\{\frac{1}{\tilde{s}_k}\right\} & \Re\left\{\frac{1}{\tilde{s}_k}\right\} \end{bmatrix} \in \mathbb{R}^{2\times 2}$, $\mathbf{H}_k \triangleq \begin{bmatrix} \Re\left\{\tilde{\mathbf{h}}_k^T\right\} & -\Im\left\{\tilde{\mathbf{h}}_k^T\right\} \\ \Im\left\{\tilde{\mathbf{h}}_k^T\right\} & \Re\left\{\tilde{\mathbf{h}}_k^T\right\} \end{bmatrix} \in \mathbb{R}^{2\times 2N_t}$. We further introduce $\bar{\mathbf{A}}_k \triangleq \mathbf{T}\mathbf{S}_k\mathbf{H}_k$, and $\mathbf{b}_k \triangleq \sqrt{\gamma_k}\sigma_k\mathbf{1}$. Accordingly, the CI constraints become $\bar{\mathbf{A}}_k\mathbf{x} \succeq \mu\mathbf{b}_k$, $\forall k$. A compact formulation can be attained by stacking the CI constraints for all K users, given by

$$\mathbf{A}\mathbf{x} \succeq \mu\mathbf{b}, \tag{9}$$

where $\mathbf{A} \triangleq \left[\bar{\mathbf{A}}_1^T, \cdots, \bar{\mathbf{A}}_K^T\right]^T \in \mathbb{R}^{2K\times 2N_t}$, $\mathbf{b} \triangleq \left[\mathbf{b}_1^T, \cdots, \mathbf{b}_K^T\right]^T \in \mathbb{R}^{2K}$. It can be seen that the left-hand side of (9) can be expressed as a linear combination of the columns of $\mathbf{A}$, i.e., $\sum_{i=1}^{2N_t} \mathbf{a}_i x_i$, where $\mathbf{a}_i$ is the i-th column of $\mathbf{A}$, x_i is the i-th entry of $\mathbf{x}$. Subsequently, (8) can be rearranged as

$$\begin{aligned} \left\{\mathbf{x}^{SB}(\mathbf{b},p), \mu^{SB}(\mathbf{b},p)\right\} = \arg\max_{\{\mathbf{x}_i\},\mu} \quad & \mu \\ \text{s.t.} \sum_{i=1}^{N} \mathbf{A}_i\mathbf{x}_i \succeq \mu\mathbf{b}, \\ \sum_{i=1}^{N} \|\mathbf{x}_i\|^2 \le p, \end{aligned} \tag{10}$$

where $\mathbf{x}_i \in \mathbb{R}^{n_i}$ with $\sum_{i=1}^{N} n_i = 2N_t$ and $\mathbf{A}_i \in \mathbb{R}^{2K\times n_i}$ are the i-th blocks of $\mathbf{x}$ and $\mathbf{A}$, respectively. $\mathbf{x}_i$ is composed of the adjacent and/or disadjacent elements of $\mathbf{x}$. Each column of $\mathbf{A}_i$ is uniquely taken from the columns of $\mathbf{A}$. Specifically, if the elements in $\mathbf{x}_i$ are taken from $\mathbf{x}$ continuously, we have $\mathbf{x} = \left[\mathbf{x}_1^T, \cdots, \mathbf{x}_N^T\right]^T$, $\mathbf{A} = [\mathbf{A}_1, \cdots, \mathbf{A}_N]$. On the other hand, if we want to group the disadjacent elements of $\mathbf{x}$ into one group, e.g., the real and imaginary parts of the same antenna, which can be expressed as $\mathbf{x}_i = \mathbf{E}_i^T\mathbf{x}$, $\mathbf{A}_i = \mathbf{A}\mathbf{E}_i$, where $\mathbf{E}_i \in \mathbb{R}^{2N_t\times n_i}$, and each column of $\{\mathbf{E}_i\}$ is uniquely picked from the columns of the $2N_t \times 2N_t$ identity matrix.

In accordance with the procedure formulating (10), the real-valued equivalent of the PM-SLP problem (5) can be rearranged as [32]

$$\begin{aligned} \mathbf{x}^{PM}(\mathbf{b}) = \arg\min_{\{\mathbf{x}_i\}} \quad & \sum_{i=1}^{N} \|\mathbf{x}_i\|^2 \\ \text{s.t.} & \sum_{i=1}^{N} \mathbf{A}_i\mathbf{x}_i \succeq \mathbf{b}. \end{aligned} \tag{11}$$

The above formulation was first proposed in our previous work [32], where the separable structure of the PM-SLP problem with PSK modulation is proved. The structure was further utilized to decompose the original problem into multiple parallel subproblems by the proposed PIF-SLP algorithm.

Contrary to the separable PM-SLP problem with PSK modulation (11), it is observed that the above SB-SLP problem (10) is not separable because of the objective function μ, which cannot be separated. Thus the PIF-SLP approach proposed in [32] is not applicable to decompose the SB-SLP problem at first glance. Fortunately, we find an explicit relation inherent in the two problems, which indicates that once the optimal solution to the PM-SLP problem is obtained via the PIF-SLP [32] or other algorithms, then finding the optimal solution to the SB-SLP problem is trivial, which is termed as the duality to be presented below.

B. Duality Between the PM-SLP and SB-SLP with PSK Modulation

For the conventional block-level interference suppression precoding, it is known that the PM problem and the SB

problem are a pair of inverse problems [13], [34]. This relationship has been extended to CI-based SLP by [16], which proposes to solve the SB-SLP problem via iteratively solving its inverse PM-SLP problem along with a bisection search. Unlike the high-complexity one-dimension search scheme, recently, a novel duality between the conventional multicast PM and SB problems has been revealed [35], which explicitly determines the solution to the SB problem given the solution to the PM problem, and vice versa. Later in CI-based symbol error rate minimization precoding, a closed-form algorithm was designed to solve the detection-region-based noise uncertainty radius maximization problem under the precondition of the solved detection-region-based PM problem [36]. In this subsection, we shall establish a novel duality between the PM-SLP and SB-SLP problems with PSK signaling.

Let $\mathbf{x}^{PM}$ and $p^{PM} \triangleq \|\mathbf{x}^{PM}\|^2$ denote the optimal solution and objective value of the PM-SLP problem with PSK modulation (11). $\mathbf{x}^{SB}$ and $\mu^{SB} \triangleq \min_i \frac{1}{\bar{b}_i}\bar{\mathbf{a}}_i^T\mathbf{x}^{SB}$ are the optimal counterparts for the SB-SLP problem in (10), where $\bar{\mathbf{a}}_i$ denotes the transpose of the i-th row of $\mathbf{A}$, and $\bar{b}_i$ represents the i-th entry of $\mathbf{b}$.

Lemma 1: For PSK modulation, the PM-SLP problem (11) and the SB-SLP problem (10) are inverse problems:

$$\mathbf{x}^{PM}(\alpha\mathbf{b}) = \mathbf{x}^{SB}\left(\mathbf{b}, p^{PM}(\alpha\mathbf{b})\right), \tag{12}$$

with $\alpha = \mu^{SB}\left(\mathbf{b}, p^{PM}(\alpha\mathbf{b})\right)$. Reciprocally,

$$\mathbf{x}^{SB}(\mathbf{b}, p) = \mathbf{x}^{PM}\left(\mu^{SB}(\mathbf{b}, p)\,\mathbf{b}\right), \tag{13}$$

with $p = p^{PM}\left(\mu^{SB}(\mathbf{b}, p)\,\mathbf{b}\right)$.

Proof: Contradiction can be used to prove (12). Assume that there exists an optimal solution $\mathbf{x}^{SB}\left(\mathbf{b}, p^{PM}(\alpha\mathbf{b})\right)$ and the corresponding optimal value $\mu^{SB}\left(\mathbf{b}, p^{PM}(\alpha\mathbf{b})\right)$ for the SB-SLP problem (10) given parameters $\mathbf{b}$ and $p^{PM}(\alpha\mathbf{b})$. Similarly, assume the optimal solution and the optimal value for the PM-SLP problem (11) given $\alpha\mathbf{b}$ are $\mathbf{x}^{PM}(\alpha\mathbf{b})$ and $p^{PM}(\alpha\mathbf{b})$, respectively. By definition, $\mathbf{x}^{PM}(\alpha\mathbf{b})$ is a feasible solution to the above SB-SLP problem, and the associated objective value is α. If $\alpha > \mu^{SB}\left(\mathbf{b}, p^{PM}(\alpha\mathbf{b})\right)$, then this is a contradiction for the optimality of $\mu^{SB}\left(\mathbf{b}, p^{PM}(\alpha\mathbf{b})\right)$. Otherwise, if $\alpha < \mu^{SB}\left(\mathbf{b}, p^{PM}(\alpha\mathbf{b})\right)$, then $\mathbf{x}^{SB}\left(\mathbf{b}, p^{PM}(\alpha\mathbf{b})\right)$ is also a feasible solution to the PM-SLP problem (11) given $\alpha\mathbf{b}$, for which all the CI constraints are over satisfied. Therefore, one can always find a $v \in (0,1)$ such that $v\mathbf{x}^{SB}\left(\mathbf{b}, p^{PM}(\alpha\mathbf{b})\right)$ meets all the CI constraints while providing a smaller objective value than $p^{PM}(\alpha\mathbf{b})$. This is a contradiction for the optimality of $p^{PM}(\alpha\mathbf{b})$. The above proves (12) is true with $\alpha = \mu^{SB}\left(\mathbf{b}, p^{PM}(\alpha\mathbf{b})\right)$. The proof of (13) is similar and is therefore omitted. ■

Lemma 2: Consider the PM-SLP problem with PSK modulation (11), for any $\alpha > 0$, we have

$$\mathbf{x}^{PM}(\alpha\mathbf{b}) = \alpha\mathbf{x}^{PM}(\mathbf{b}), \tag{14}$$

$$p^{PM}(\alpha\mathbf{b}) = \alpha^2 p^{PM}(\mathbf{b}). \tag{15}$$

For the SB-SLP problem (10), we have

$$\mathbf{x}^{SB}\left(\mathbf{b}, \alpha^2 p\right) = \alpha\mathbf{x}^{SB}(\mathbf{b}, p), \tag{16}$$

$$\mu^{SB}\left(\mathbf{b}, \alpha^2 p\right) = \alpha\mu^{SB}(\mathbf{b}, p). \tag{17}$$

Proof: Let $\mathbf{x} = \frac{\dot{\mathbf{x}}}{\alpha}$, where $\alpha > 0$, $\dot{\mathbf{x}} = \alpha\mathbf{x}$. Replacing $\mathbf{x}$ in (11) yields

$$\begin{aligned} \min_{\{\dot{\mathbf{x}}_i\}} \quad & \sum_{i=1}^{N} \|\dot{\mathbf{x}}_i\|^2 \\ \text{s.t.} \quad & \sum_{i=1}^{N} \mathbf{A}_i\dot{\mathbf{x}}_i \succeq \alpha\mathbf{b}, \end{aligned} \tag{18}$$

then (14) and (15) follow immediately.

By substituting $\mathbf{x} = \frac{\dot{\mathbf{x}}}{\alpha}$ into (10), we similarly obtain

$$\begin{aligned} \max_{\{\dot{\mathbf{x}}_i\},\mu} \quad & \alpha\mu \\ \text{s.t.} \quad & \sum_{i=1}^{N} \mathbf{A}_i\dot{\mathbf{x}}_i \succeq \alpha\mu\mathbf{b}, \\ & \sum_{i=1}^{N} \|\dot{\mathbf{x}}_i\|^2 \le \alpha^2 p, \end{aligned} \tag{19}$$

which induces (16) and (17). ■

Theorem 1 (Duality for PSK Modulation): Let $\mathbf{x}^{PM}$ and $p^{PM} \triangleq \|\mathbf{x}^{PM}\|^2$ denote the optimal solution and the optimal value of the PM-SLP problem (11), respectively. Then the counterparts of the SB-SLP problem, $\mathbf{x}^{SB}$ and μ^{SB}, are determined as

$$\mathbf{x}^{SB}(\mathbf{b}, p) = \sqrt{\frac{p}{p^{PM}(\mathbf{b})}}\mathbf{x}^{PM}(\mathbf{b}), \tag{20}$$

$$\mu^{SB}(\mathbf{b}, p) = \sqrt{\frac{p}{p^{PM}(\mathbf{b})}}. \tag{21}$$

and vice versa as

$$\mathbf{x}^{PM}(\mathbf{b}) = \frac{1}{\mu^{SB}(\mathbf{b}, p)}\mathbf{x}^{SB}(\mathbf{b}, p), \tag{22}$$

$$p^{PM}(\mathbf{b}) = \frac{p}{\left(\mu^{SB}(\mathbf{b}, p)\right)^2}. \tag{23}$$

Proof: The optimal solution to the SB-SLP problem can be equivalently written as

$$\mathbf{x}^{SB}(\mathbf{b}, p) = \mathbf{x}^{SB}\left(\mathbf{b}, \frac{p}{p^{PM}(\mathbf{b})}p^{PM}(\mathbf{b})\right). \tag{24}$$

By using (15) to transfer the transmit power budget in (24), we have

$$\begin{aligned} &\mathbf{x}^{SB}\left(\mathbf{b}, \frac{p}{p^{PM}(\mathbf{b})}p^{PM}(\mathbf{b})\right) \\ &\qquad = \mathbf{x}^{SB}\left(\mathbf{b}, p^{PM}\left(\sqrt{\frac{p}{p^{PM}(\mathbf{b})}}\mathbf{b}\right)\right). \end{aligned} \tag{25}$$

Combining (25) with (12) yields

$$\mathbf{x}^{SB}\left(\mathbf{b}, p^{PM}\left(\sqrt{\frac{p}{p^{PM}(\mathbf{b})}}\mathbf{b}\right)\right) = \mathbf{x}^{PM}\left(\sqrt{\frac{p}{p^{PM}(\mathbf{b})}}\mathbf{b}\right). \tag{26}$$

From (14) we have

$$\mathbf{x}^{PM}\left(\sqrt{\frac{p}{p^{PM}(\mathbf{b})}}\mathbf{b}\right) = \sqrt{\frac{p}{p^{PM}(\mathbf{b})}}\mathbf{x}^{PM}(\mathbf{b}). \tag{27}$$

Hence (20) is true.

We then use Lemma 1 and Lemma 2 to prove (21) and (23). It is shown in Lemma 1 that

$$p = p^{PM}\left(\mu^{SB}\left(\mathbf{b}, p\right)\mathbf{b}\right). \tag{28}$$

Using (15), the above equality yields

$$p^{PM}\left(\mu^{SB}\left(\mathbf{b}, p\right)\mathbf{b}\right) = \left(\mu^{SB}\left(\mathbf{b}, p\right)\right)^2 p^{PM}\left(\mathbf{b}\right). \tag{29}$$

Thus (21) and (23) follow immediately.

The proof of (22) is similar to that of (20). For brevity, we give an abbreviated proof below:

$$\begin{aligned}
\mathbf{x}^{PM}\left(\mathbf{b}\right) &= \mathbf{x}^{PM}\left(\frac{1}{\mu^{SB}\left(\mathbf{b}, p\right)}\mu^{SB}\left(\mathbf{b}, p\right)\mathbf{b}\right) \\
&\overset{(17)}{=} \mathbf{x}^{PM}\left(\mu^{SB}\left(\mathbf{b}, \frac{1}{\left(\mu^{SB}\left(\mathbf{b}, p\right)\right)^2}p\right)\mathbf{b}\right) \\
&\overset{(13)}{=} \mathbf{x}^{SB}\left(\mathbf{b}, \frac{1}{\left(\mu^{SB}\left(\mathbf{b}, p\right)\right)^2}p\right) \\
&\overset{(16)}{=} \frac{1}{\mu^{SB}\left(\mathbf{b}, p\right)}\mathbf{x}^{SB}\left(\mathbf{b}, p\right).
\end{aligned} \tag{30}$$

■

Corollary 1: The SB-SLP problem and the PM-SLP problem can be solved simultaneously. In particular, the solution to the SB-SLP problem (10) can be obtained by first solving the PM-SLP problem (11) and then scaling the transmit power to satisfy the power budget of the SB-SLP problem, and vice versa.

C. Power Scaling Algorithm

According to Corollary 1, the SB-SLP problem with PSK modulation can be solved by a simple one-step power scaling algorithm, provided that the solution to the PM-SLP problem is available. Specifically, we solve (11) by the PIF-SLP [32] or other algorithms and obtain $\mathbf{x}^{PM}(\mathbf{b})$ as well as $p^{PM}(\mathbf{b})$, then compute the solution to SB-SLP by (20), which is termed the power scaling algorithm for SLP. The proposed closed-form power scaling algorithm is summarized in Algorithm 1. We point out that although the parallel algorithm cannot directly be applied to the SB-SLP problem due to the lack of separability, a SPIF-SLP algorithm can be designed to solve the SB-SLP problem with the aid of the closed-form power scaling algorithm, which consists of two steps. In the first step, we obtain the parallelizable solution to the PM-SLP problem via the PIF-SLP algorithm proposed in [32]. Whileas in the second step, we use the closed-form power scaling algorithm to acquire the solution to the SB-SLP problem. By applying the PIF-SLP algorithm along with the closed-form power scaling algorithm, the separability of the PM-SLP problem can be utilized to attain a low-complexity and parallelizable solution to the SB-SLP problem.

IV. Proposed Parallelizable CI-SLP Algorithms for QAM Modulation

In this section, we address the PM-SLP and SB-SLP problems with QAM modulation. Other multi-level modulations such as amplitude phase shift keying (APSK) can be analyzed with a similar methodology.

Algorithm 1 Power Scaling Algorithm for the SB-SLP Problem (10)

Input: $\mathbf{A}$, $\mathbf{b}$, p
Output: $\mathbf{x}$

1: Solve (11) by the PIF-SLP [32] or other algorithms, obtain $\mathbf{x}^{PM}(\mathbf{b})$ and $p^{PM}(\mathbf{b})$;
2: Compute $\mathbf{x}$ by (20).

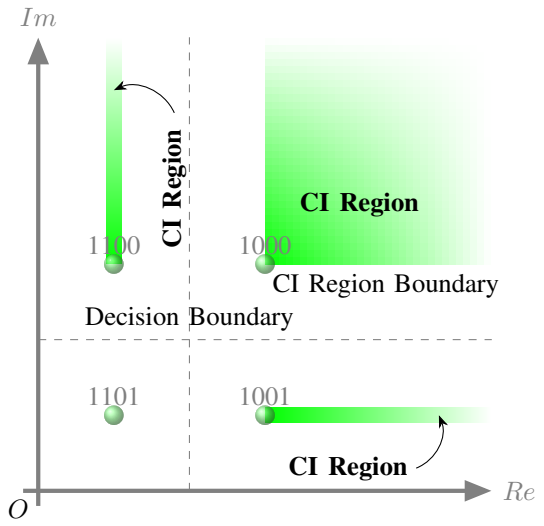

Fig. 2. Illustration of CI regions for the first quadrant of the 16QAM constellation.

To begin with, the first quadrant of a 16QAM constellation is depicted in Fig. 2 as an example, from which we can observe that only the inner constellation point '1101' has a closed or fully-bounded decision region, and the other three constellation points have open decision regions bounded by either two or three decision boundaries. The three green-shaded areas associated with '1001', '1100', and '1000' are CI regions. One of the main differences between multi-level and constant-envelope modulations is whether the constellation point has closed decision regions or not. From Fig. 2 we can conclude that only the data symbols corresponding to open decision boundaries have degrees of freedom to exploit CI. Specifically, the open decision regions bounded by two and three decision boundaries have two and one dimensions to exploit CI, respectively. For the inner constellation points, we cannot push them away from one decision boundary while preserving the distance to another decision boundary. Therefore, as shown in Fig. 2, the left-edge constellation point '1001' has its real part to exploit CI, and the upper-edge constellation point '1100' has its imaginary part to exploit CI. The corresponding CI regions are two rays. On the other hand, the vertex constellation point '1000' has both real and imaginary parts to exploit CI. Consequently, its CI region is a two-dimensional convex polyhedron similar to PSK modulation.

The mathematical formulation of CI constraints such that

the noiseless received signal lies in the CI region and meets the instantaneous SINR threshold γ_k for QAM signaling can be written as

$$sign\left\{\Re\left\{\tilde{s}_k\right\}\right\}\Re\left\{\tilde{\mathbf{h}}_k^T\tilde{\mathbf{x}}\right\} \trianglerighteq sign\left\{\Re\left\{\tilde{s}_k\right\}\right\}\sqrt{\gamma_k}\sigma_k\Re\left\{\tilde{s}_k\right\}, \quad \forall k, \quad (31)$$

$$sign\left\{\Im\left\{\tilde{s}_k\right\}\right\}\Im\left\{\tilde{\mathbf{h}}_k^T\tilde{\mathbf{x}}\right\} \trianglerighteq sign\left\{\Im\left\{\tilde{s}_k\right\}\right\}\sqrt{\gamma_k}\sigma_k\Im\left\{\tilde{s}_k\right\}, \quad \forall k, \quad (32)$$

where $\trianglerighteq$ represents the generalized inequality symbol, i.e., $\trianglerighteq$ equals to $\geq$ or $=$, depending on whether CI can be exploited or not. By introducing $\hat{\mathbf{h}}_k^T \triangleq \frac{\tilde{\mathbf{h}}_k^T}{\tilde{s}_k}$, the above original CI constraints can be rearranged as

$$\Re\left\{\hat{\mathbf{h}}_k^T\tilde{\mathbf{x}}\right\} \trianglerighteq \sqrt{\gamma_k}\sigma_k, \forall k, \quad (33)$$

$$\Im\left\{\hat{\mathbf{h}}_k^T\tilde{\mathbf{x}}\right\} \trianglerighteq \sqrt{\gamma_k}\sigma_k, \forall k. \quad (34)$$

It is worth noting that this is a succinct and easy-to-handle formulation that differs from the existing literature [24], [25], [29].

A. Problem Formulation

1) PM-SLP Problem: The PM-SLP problem with QAM modulation that minimizes the total transmit power subject to CI constraints can be formulated as

$$\begin{aligned}\min_{\tilde{\mathbf{x}}} \quad & \left\|\tilde{\mathbf{x}}\right\|^2 \\ \text{s.t.}\ & \Re\left\{\hat{\mathbf{h}}_k^T\tilde{\mathbf{x}}\right\} \trianglerighteq \sqrt{\gamma_k}\sigma_k, \forall k, \\ & \Im\left\{\hat{\mathbf{h}}_k^T\tilde{\mathbf{x}}\right\} \trianglerighteq \sqrt{\gamma_k}\sigma_k, \forall k.\end{aligned} \quad (35)$$

Although the EGPA proposed in [15] was designed only for PSK modulation, it can be used to solve the above problem with proper modification. The suboptimal closed-form solution proposed in [26] and the improved suboptimal closed-form solution proposed in [27] can also be employed to obtain suboptimal solutions to the above problem.

2) SB-SLP Problem: The SB-SLP problem with QAM modulation aims to maximize the minimum instantaneous SINR in CI regions subject to a total transmit power constraint. Like in the PSK modulation case, this problem can also be rewritten in a SOCP form given by

$$\begin{aligned}\max_{\tilde{\mathbf{x}},\mu} \quad & \mu \\ \text{s.t.}\ & \frac{1}{\sqrt{\gamma_k}}\Re\left\{\hat{\mathbf{h}}_k^T\tilde{\mathbf{x}}\right\} \trianglerighteq \mu\sigma_k, \forall k, \\ & \frac{1}{\sqrt{\gamma_k}}\Im\left\{\hat{\mathbf{h}}_k^T\tilde{\mathbf{x}}\right\} \trianglerighteq \mu\sigma_k, \forall k, \\ & \left\|\tilde{\mathbf{x}}\right\|^2 \leq p,\end{aligned} \quad (36)$$

where p denotes the total transmit power budget, $\frac{1}{\sqrt{\gamma_k}}$ denotes the square-root of the weight of SINR_k. Following the iterative algorithm for the SB-SLP problem with PSK modulation [28], a modified iterative algorithm, as well as a suboptimal closed-form solution, were subsequently developed for the above problem [29].

B. Separability of the PM-SLP with QAM Modulation

The real-valued equivalent of (35) is given by

$$\begin{aligned}\min_{\mathbf{x}} \quad & \left\|\mathbf{x}\right\|^2 \\ \text{s.t.}\ & \mathbf{S}_k\mathbf{H}_k\mathbf{x} \trianglerighteq \sqrt{\gamma_k}\sigma_k\mathbf{1}, \forall k,\end{aligned} \quad (37)$$

where $\mathbf{x}$, $\mathbf{S}_k$, and $\mathbf{H}_k$ have the same values as those in the PSK case. It can be seen that the above PM-SLP problem formulation for QAM modulation is equivalent to its counterpart for QPSK modulation, except for the generalized inequality symbol. This is because the four vertex constellation points in a square QAM constellation can be viewed as a QPSK constellation. The above problem can be rearranged to a separable formulation, given by

$$\begin{aligned}\mathbf{x}^{PM}\left(\mathbf{b}\right) = \arg\min_{\{\mathbf{x}_i\}} \quad & \sum_{i=1}^{N}\left\|\mathbf{x}_i\right\|^2 \\ \text{s.t.}\ & \sum_{i=1}^{N}\mathbf{A}_i\mathbf{x}_i \trianglerighteq \mathbf{b},\end{aligned} \quad (38)$$

where the notations directly inherent from the PSK case, except for $\mathbf{A} \triangleq \left[\bar{\mathbf{A}}_1^T, \cdots, \bar{\mathbf{A}}_K^T\right]^T \in \mathbb{R}^{2K\times 2N_t}$, $\bar{\mathbf{A}}_k \triangleq \mathbf{S}_k\mathbf{H}_k$. Accordingly, the optimization variable $\mathbf{x}$ is split into N separate subvectors. In addition, the objective function and constraints of the PM-SLP problem with QAM modulation can also be written as summations of N individual blocks, each of which only associates with a subvector of $\mathbf{x}$. This indicates that the problem is separable, similar to the PSK case. Decomposition methods are therefore applicable to partition the problem into smaller separate subproblems, each of which can be updated in a sequential or parallel, centralized or decentralized manner.

C. Parallel Inverse-Free Algorithm for PM-SLP with QAM Modulation

This subsection develops a PIF-SLP algorithm for the PM-SLP problem with QAM modulation taking advantage of its separability presented in the previous subsection. Although sharing the same name with our previous work in [32] because they have the same parallelizable and inversion-free properties, this algorithm is different from the previous one. The reason lies in that we have to tackle both the inequality and equality constraints corresponding to the outer and inner constellation points for QAM modulation, which leads to a different feasible region for the Lagrangian multiplier compared to the PSK case.

To start with, we reformulate (38) by introducing a slack variable vector $\mathbf{c}$ to convert the original generalized inequality constraints into corresponding equality constraints as follows:

$$\begin{aligned}\min_{\{\mathbf{x}_i\},\mathbf{c}} \quad & \sum_{i=1}^{N}\left\|\mathbf{x}_i\right\|^2 \\ \text{s.t.}\ & \sum_{i=1}^{N}\mathbf{A}_i\mathbf{x}_i = \mathbf{b}+\mathbf{c}, \\ & \mathbf{c} \in \mathcal{C},\end{aligned} \quad (39)$$

$$\begin{aligned}\mathcal{L}_\rho(\mathbf{x},\mathbf{c},\boldsymbol{\lambda}) &= \sum_{i=1}^{N}\|\mathbf{x}_i\|^2 + \mathcal{I}_{\mathcal{C}}(\mathbf{c}) + \boldsymbol{\lambda}^T\left(-\sum_{i=1}^{N}\mathbf{A}_i\mathbf{x}_i+\mathbf{b}+\mathbf{c}\right) + \frac{\rho}{2}\left\|-\sum_{i=1}^{N}\mathbf{A}_i\mathbf{x}_i+\mathbf{b}+\mathbf{c}\right\|^2 \\ &= \sum_{i=1}^{N}\|\mathbf{x}_i\|^2 + \mathcal{I}_{\mathcal{C}}(\mathbf{c}) + \frac{\rho}{2}\left\|-\sum_{i=1}^{N}\mathbf{A}_i\mathbf{x}_i+\mathbf{b}+\mathbf{c}+\frac{\boldsymbol{\lambda}}{\rho}\right\|^2 - \frac{1}{2\rho}\|\boldsymbol{\lambda}\|^2 \end{aligned} \tag{42}$$

where $\mathcal{C} \triangleq \left\{\mathbf{c}\middle| c_i \geq 0, \forall i \in \mathcal{W}; c_j = 0, \forall j \neq i\right\} \subseteq \mathbb{R}^{2K}$ is the feasible region of $\mathbf{c}$, where $\mathcal{W} \triangleq \left\{i\middle||s_i| = \|\mathbf{w}\|_\infty\right\}$, $\mathbf{s} \triangleq [\Re\{\tilde{s}_1\}, \Im\{\tilde{s}_1\}, \cdots, \Re\{\tilde{s}_K\}, \Im\{\tilde{s}_K\}]^T$, c_i and s_i are the i-th entries of $\mathbf{c}$ and $\mathbf{s}$, respectively. Assume $\mathbf{w} \triangleq [\Re\{\tilde{w}_1\}, \Im\{\tilde{w}_1\}, \cdots, \Re\{\tilde{w}_{\mathcal{M}}\}, \Im\{\tilde{w}_{\mathcal{M}}\}]^T$ is composed of the real and imaginary parts of all the constellation points of a square $\mathcal{M}$-QAM constellation. The feasible constraint of the slack variable $\mathbf{c}$ can be further incorporated into the objective function:

$$\begin{aligned}\min_{\{\mathbf{x}_i\},\mathbf{c}} \quad & \sum_{i=1}^{N}\|\mathbf{x}_i\|^2 + \mathcal{I}_{\mathcal{C}}(\mathbf{c}) \\ \text{s.t.} \quad & -\sum_{i=1}^{N}\mathbf{A}_i\mathbf{x}_i+\mathbf{b}+\mathbf{c}=\mathbf{0},\end{aligned} \tag{40}$$

where $\mathcal{I}_{\mathcal{C}}(\mathbf{c})$ is the indicator function of $\mathcal{C}$ given by

$$\mathcal{I}_{\mathcal{C}}(\mathbf{c}) = \begin{cases}0, & \text{if } \mathbf{c}\in\mathcal{C},\\ +\infty, & \text{otherwise.}\end{cases} \tag{41}$$

The augmented Lagrangian function of (40) is presented in (42) on the top of the next page, where $\boldsymbol{\lambda}$ represents the Lagrangian multiplier, ρ is a penalty parameter that tunes the severity of the quadratic penalty on constraint violations.

In line with the PJ-ADMM framework [32], [37], the standard PJ-ADMM iterations that minimize the augmented Lagrangian function of the PM-SLP problem with QAM modulation are

$$\mathbf{c}^{t+1} = \arg\min_{\mathbf{c}} \mathcal{L}_\rho\left(\mathbf{x}_1^t,\cdots,\mathbf{x}_N^t,\mathbf{c},\boldsymbol{\lambda}^t\right), \tag{43a}$$

$$\mathbf{x}_i^{t+1} = \arg\min_{\mathbf{x}_i} \mathcal{L}_\rho\left(\mathbf{x}_{\neq i}^t,\mathbf{x}_i,\mathbf{c}^{t+1},\boldsymbol{\lambda}^t\right) + \frac{1}{2}\left\|\mathbf{x}_i-\mathbf{x}_i^t\right\|_{\mathbf{P}_i}^2, \forall i, \tag{43b}$$

$$\boldsymbol{\lambda}^{t+1} = \boldsymbol{\lambda}^t + \beta\rho\left(-\sum_{i=1}^{N}\mathbf{A}_i\mathbf{x}_i^{t+1}+\mathbf{b}+\mathbf{c}^{t+1}\right), \tag{43c}$$

where $\beta > 0$ is a damping parameter, $\mathbf{P}_i$ is a symmetric and positive semi-definite matrix that determines the degree of proximity between two consecutive iterations of the transmit signal and $\|\mathbf{x}_i\|_{\mathbf{P}_i}^2 \triangleq \mathbf{x}_i^T\mathbf{P}_i\mathbf{x}_i$. The value of $\mathbf{P}_i$ is experimentally determined in practice.[1]

It can be observed from (43) that the update of the Lagrangian multiplier $\boldsymbol{\lambda}$ in (43c) uses the outdated slack variable. We can update the slack variable $\mathbf{c}$ twice at each iteration to obtain a more accurate slack variable for the Lagrangian multiplier, which is beneficial for convergence. With such a mechanism, the updates of the primal variable $\mathbf{x}$ and the dual variable $\boldsymbol{\lambda}$ are symmetric with respect to the update of the slack variable in the sense that they are both followed by the update of the slack variable. The slack variable-symmetric PJ-ADMM iterations are given by

$$\mathbf{c}^{t+\frac{1}{2}} = \arg\min_{\mathbf{c}} \mathcal{L}_\rho\left(\mathbf{x}_1^t,\cdots,\mathbf{x}_N^t,\mathbf{c},\boldsymbol{\lambda}^t\right), \tag{44a}$$

$$\mathbf{x}_i^{t+1} = \arg\min_{\mathbf{x}_i} \mathcal{L}_\rho\left(\mathbf{x}_{\neq i}^t,\mathbf{x}_i,\mathbf{c}^{t+\frac{1}{2}},\boldsymbol{\lambda}^t\right) + \frac{1}{2}\left\|\mathbf{x}_i-\mathbf{x}_i^t\right\|_{\mathbf{P}_i}^2, \forall i, \tag{44b}$$

$$\mathbf{c}^{t+1} = \arg\min_{\mathbf{c}} \mathcal{L}_\rho\left(\mathbf{x}_1^{t+1},\cdots,\mathbf{x}_N^{t+1},\mathbf{c},\boldsymbol{\lambda}^t\right), \tag{44c}$$

$$\boldsymbol{\lambda}^{t+1} = \boldsymbol{\lambda}^t + \beta\rho\left(-\sum_{i=1}^{N}\mathbf{A}_i\mathbf{x}_i^{t+1}+\mathbf{b}+\mathbf{c}^{t+1}\right). \tag{44d}$$

Based on the above derivations, the original PM-SLP problem with QAM modulation is decomposed into multiple subproblems that can be calculated in a parallel and distributed manner with (43) or (44). In what follows, we shall derive closed-form solutions for each subproblem in the standard PJ-ADMM iterations.

The update for the slack variable $\mathbf{c}$ can be written as

$$\mathbf{c}^{t+1} = \arg\min_{\mathbf{c}\in\mathcal{C}} \frac{\rho}{2}\left\|-\sum_{i=1}^{N}\mathbf{A}_i\mathbf{x}_i^t+\mathbf{b}+\mathbf{c}+\frac{\boldsymbol{\lambda}^t}{\rho}\right\|^2, \tag{45}$$

which is equivalent to projecting the vector $\sum_{i=1}^{N}\mathbf{A}_i\mathbf{x}_i^t-\mathbf{b}-\frac{\boldsymbol{\lambda}^t}{\rho}$ onto $\mathcal{C}$, denoted by $\Pi_{\mathcal{C}}\left(\sum_{i=1}^{N}\mathbf{A}_i\mathbf{x}_i^t-\mathbf{b}-\frac{\boldsymbol{\lambda}^t}{\rho}\right)$. Its closed-form solution is given by

$$\mathbf{c}_j^{t+1} = \begin{cases}\max\left\{\sum_{i=1}^{N}\bar{\mathbf{A}}_i^j\mathbf{x}_i^t - b_j - \frac{\lambda_j^t}{\rho}, 0\right\}, & \text{if } j\in\mathcal{W},\\ 0, & \text{otherwise,}\end{cases} \tag{46}$$

where $\bar{\mathbf{A}}_i^j$ represents the j-th row of $\mathbf{A}_i$. b_j and λ_j^t are the j-th entries of b_j and λ_j^t, respectively.

The iteration for $\mathbf{x}_i^{t+1}$ is updated as follows:

$$\begin{aligned}\mathbf{x}_i^{t+1} = \arg\min_{\mathbf{x}_i} \ & \|\mathbf{x}_i\|^2 \\ & + \frac{\rho}{2}\left\|-\mathbf{A}_i\mathbf{x}_i-\sum_{j\neq i}^{N}\mathbf{A}_j\mathbf{x}_j^t+\mathbf{b}+\mathbf{c}^{t+1}+\frac{\boldsymbol{\lambda}^t}{\rho}\right\|^2 \\ & + \frac{1}{2}\left\|\mathbf{x}_i-\mathbf{x}_i^t\right\|_{\mathbf{P}_i}^2, \forall i,\end{aligned} \tag{47}$$

[1]There are two special cases of the proximal matrix: 1) $\mathbf{P}_i = \tau_i\mathbf{I}$; 2) $\mathbf{P}_i = \tau_i\mathbf{I} - \rho\mathbf{A}_i^T\mathbf{A}_i$. The second case will be discussed at the end of this subsection. More detailed discussion on the value of $\mathbf{P}_i$, please refer to [32].

Algorithm 2 PIF-SLP Algorithm for the PM-SLP Problem with QAM Modulation (38)

Input: $\mathbf{A}$, $\mathbf{b}$, ρ, $\{\tau_i\}$, β
Output: $\mathbf{x}$

```
Initialize x_i^0 (i = 1, ..., N), and λ^0;
Set t ← 0;
repeat
  for t = 0, 1, ... do
    Update c^{t+1/2} by (46);
    Update x_i^{t+1} for i = 1, ..., N in parallel by:
    for i = 1, ..., N do
      Update x_i^{t+1} by (50);
    end for
    Update c^{t+1} by (46);
    Update λ^{t+1} by (44d));
    Set t ← t + 1;
  end for
until Convergence.
```

which admits a closed-form solution by setting the gradient of the objective function with respect to $\mathbf{x}_i$ to zero. The closed-form solution for $\mathbf{x}_i^{t+1}$ can be written as

$$\mathbf{x}_i^{t+1} = \left(2\mathbf{I} + \rho\mathbf{A}_i^T\mathbf{A}_i + \mathbf{P}_i\right)^{-1} \left[\mathbf{P}_i\mathbf{x}_i^t \times \left(-\sum_{j\neq i}^{N}\mathbf{A}_j\mathbf{x}_j^t + \mathbf{b} + \mathbf{c}^{t+1} + \frac{\boldsymbol{\lambda}^t}{\rho}\right)\right], \forall i. \quad (48)$$

As proposed in [32], if we take $N = 2N_t$, then the transmit signal vector $\mathbf{x}$ is decomposed into $2N_t$ scalars, thus $\mathbf{A}_i$ reduces to a column vector $\mathbf{a}_i$, and $\mathbf{P}_i$ reduces to a scalar p_i. The update of the transmit signal can be carried out via $2N_t$ parallel and distributed scalar operations, i.e.,

$$x_i^{t+1} = \frac{p_i x_i^t + \rho\mathbf{a}_i^T\left(-\sum_{j\neq i}^{2N_t}\mathbf{a}_j x_j^t + \mathbf{b} + \mathbf{c}^{t+1} + \frac{\boldsymbol{\lambda}^t}{\rho}\right)}{2 + \rho\mathbf{a}_i^T\mathbf{a}_i + p_i}, \forall i. \quad (49)$$

To further reduce the complexity by circumventing matrix inversion of arbitrary block size as proposed in [32], $\mathbf{P}_i$ is set to $\mathbf{P}_i = \tau_i\mathbf{I} - \rho\mathbf{A}_i^T\mathbf{A}_i$. Accordingly, the parallel inverse-free update of $\mathbf{x}_i$ is given by

$$\mathbf{x}_i^{t+1} = \frac{1}{2+\tau_i} \times \left[\tau_i\mathbf{x}_i^t + \rho\mathbf{A}_i^T\left(-\sum_{i=1}^{N}\mathbf{A}_i\mathbf{x}_i^t + \mathbf{b} + \mathbf{c}^{t+1} + \frac{\boldsymbol{\lambda}^t}{\rho}\right)\right], \forall i. \quad (50)$$

Consequently, we arrive at a PIF-SLP algorithm for the PM-SLP problem with QAM modulation, which is summarized in Algorithm 2.

D. Duality between the PM-SLP and SB-SLP with QAM Modulation

In this subsection, we present the duality between the PM-SLP and SB-SLP problems with QAM modulation. To begin with, the real-valued equivalent of the SB-SLP problem with QAM modulation (36) can be rearranged as

$$\left\{\mathbf{x}^{SB}(\mathbf{b},p), \mu^{SB}(\mathbf{b},p)\right\} = \arg\max_{\{\mathbf{x}_i\},\mu} \quad \mu \quad \text{s.t.} \sum_{i=1}^{N}\mathbf{A}_i\mathbf{x}_i \succeq \mu\mathbf{b}, \quad \sum_{i=1}^{N}\|\mathbf{x}_i\|^2 \leq p. \quad (51)$$

The above formulation implies that the SB-SLP problem with QAM modulation is not separable. Recall that we proved an explicit duality between the PM-SLP and SB-SLP problems with PSK modulation in Section III and further proposed a closed-form power scaling algorithm for the SB-SLP problem with PSK modulation. Next, we shall elaborate on the same duality for QAM modulation.

Theorem 2 (Duality for QAM Modulation): The proposed explicit duality for PSK modulation in Theorem 1 can be generalized to QAM modulation.

Proof: Verbatim to the proof of Theorem 1. ■

Corollary 2: In accordance with the PSK modulation case, the SB-SLP and PM-SLP problems with QAM modulation can also be solved simultaneously. In particular, the optimal solution to the SB-SLP problem (51) can be obtained by first solving the PM-SLP problem (38) and then scaling the transmit power to satisfy the power budget of the SB-SLP problem, and vice versa.

According to Corollary 2, it is also feasible to solve the SB-SLP problem with QAM modulation via the closed-form power scaling algorithm, provided that the solution to the PM-SLP problem is given. In the previous section, we developed the PIF-SLP algorithm by taking advantage of the separable structure of the PM-SLP problem with QAM modulation, which can be connected with the power scaling algorithm to solve the SB-SLP problem. Therefore, we arrive at the SPIF-SLP algorithm for QAM modulation.

V. Computational Complexity

The computational overhead of the proposed PIF-SLP algorithm for QAM modulation outlined in Algorithm 2 and the closed-form power scaling algorithm summarized in Algorithm 1 is assessed by accounting for the required float-point operations, i.e., flops. To simplify the analysis, it is assumed that each block of transmit signal has the same dimension, which means that the transmit signal can be decomposed into N subvectors, each with $2N_t/N$ elements. Define the flop-count operator $\mathcal{F}(\mathbf{z}|\mathbf{y})$ as the number of flops to compute $\mathbf{z}$ given $\mathbf{y}$. As a result, Algorithm 2 costs

$$\begin{aligned}\mathcal{F}\left(\boldsymbol{\lambda}^{t+1}|\boldsymbol{\lambda}^t\right) &= \mathcal{F}\left(\mathbf{c}^{t+\frac{1}{2}}|\left\{\mathbf{A}_i\mathbf{x}_i^t, \boldsymbol{\lambda}^t\right\}\right) \\ &\quad + \mathcal{F}\left(\mathbf{A}_i\mathbf{x}_i^{t+1}|\left\{\mathbf{A}_i\mathbf{x}_i^t, \mathbf{c}^{t+\frac{1}{2}}, \boldsymbol{\lambda}^t\right\}\right) \\ &\quad + \mathcal{F}\left(\mathbf{c}^{t+1}|\left\{\mathbf{A}_i\mathbf{x}_i^{t+1}, \boldsymbol{\lambda}^t\right\}\right) \\ &\quad + \mathcal{F}\left(\boldsymbol{\lambda}^{t+1}|\left\{\boldsymbol{\lambda}^t, \mathbf{A}_i\mathbf{x}_i^{t+1}, \mathbf{c}^{t+1}\right\}\right) \\ &= \mathcal{O}(2K) + \mathcal{O}((2K+1)2N_t/N) \\ &\quad + \mathcal{O}(2K) + \mathcal{O}(2K) \end{aligned} \quad (52)$$

This article has been accepted for publication in IEEE Transactions on Communications. This is the author's version which has not been fully edited and content may change prior to final publication. Citation information: DOI 10.1109/TCOMM.2023.3308149

flops per iteration. As for the closed-form power scaling algorithm for the SB-SLP problem, (20) requires $\mathcal{O}(2N_t)$ flops.

VI. Simulation Results

In this section, numerical simulations are conducted to evaluate the performance of the proposed SPIF-SLP algorithm for the SB-SLP problem with PSK modulation. Additionally, the performance of both the proposed PIF-SLP algorithm and the SPIF-SLP algorithm for the PM-SLP and SB-SLP problems with QAM modulation are evaluated separately. Without loss of generality, QPSK and 16QAM are chosen as representative schemes for PSK and QAM modulations, respectively. The i.i.d. data symbols in $\tilde{\mathbf{s}}$ are drawn from the normalized QPSK constellation, i.e., $\mathcal{M} = 4$ or 16QAM constellation, i.e., $\mathcal{M} = 16$. We use '$K \times N_t$' to denote a downlink system with K single-antenna users and an N_t-antenna BS. For both PIF-SLP and SPIF-SLP in all the considered scenarios, we choose $\tau_i = \tau = 0.8\rho \left\|\mathbf{A}\right\|^2, \forall i$. The damping parameter β is set to 1. Unless otherwise specified, the penalty parameter ρ is set to 0.3, 0.4, 0.06, and 0.03 for 8×8, 12×12, 12×16, and 24×32 MU-MISO configurations, respectively. For the SB-SLP problem simulations, the square roots of the weights $\frac{1}{\sqrt{\gamma_k}}$ are all set to 1. The symmetric PJ-ADMM iterations are employed for all the simulations in this section. We assume each random channel realization is used to transmit one frame of data symbols, where a frame length is 10 ms, a symbol slot duration is 0.5 ms, and each frame contains $N_s = 20$ symbol slots. Note that implementing the proposed parallelizable algorithms in physical parallel processing units is beyond the scope of this work. However, if we use the *for* or *parfor* loop in MATLAB to simulate the low-complexity parallel procedure for the considered scenarios, the loop itself will cost a big portion of time due to sequential implementation or parallelization overheads. Therefore we set $N = 1$ in this section.

For the simulations of the SB-SLP problem, the benchmark schemes include the RZF precoding [9], the conventional linear SB-BLP solved by the fixed-point method [13], the SB-SLP solved by CVX [38], and the closed-form solutions for CI precoding (CI-CF) [28]. For the simulations of the PM-SLP problem, the results are compared with those of the ZF precoding [8], the conventional linear PM-BLP based on fixed point method [13], the IPM implemented by the CVX software package [38], and the EGPA proposed in [15].

To demonstrate the convergence of the proposed SPIF-SLP algorithm for PSK modulation, we first study its bit error rate (BER) performance as a function of the number of iterations, the results are averaged over 2000 symbol slots, where the number of random channel realizations $N_c = 100$. The benchmark scheme is the IPM implemented by the CVX software package [38]. Fig. 3 presents the BER results for the aforementioned four MU-MISO configurations. The required number of iterations for the BER of the SPIF-SLP algorithm converging to that of the CVX is about $T = 40$ for the two considered under-loaded MU-MISO configurations. The acquired number of iterations for convergence is used in the remaining under-loaded simulations for PSK modulation. On the other hand, fully-loaded MU-MISO configurations take more iterations to converge due to the symmetric channel. It is worth noting that the number of iterations for convergence varies in each fully-loaded simulation. Additionally, it is observed that the early termination of SPIF can result in a trade-off between complexity and performance.

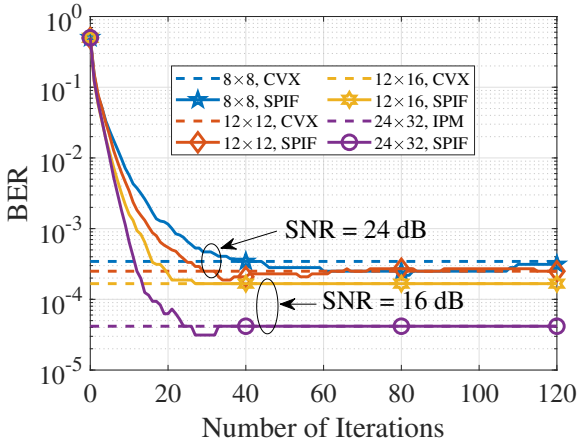

Fig. 3. BER versus number of iterations, SNR $= 24$ dB for fully-loaded systems, SNR $= 16$ dB for under-loaded systems, $N_c = 100$, $N_s = 20$, QPSK.

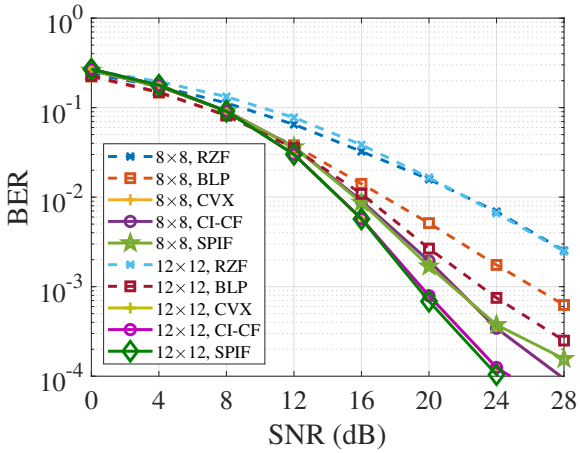

Fig. 4. BER versus SNR for two fully-loaded MU-MISO configurations, $\Delta < 1\times 10^{-3}$, $T_{max} = 100$, $N_c = 100$, $N_s = 20$, QPSK.

We then assess the BER performance versus SNR, as well as the time complexity in terms of the average execution time, of the proposed SPIF-SLP algorithm for PSK modulation. For the SB-SLP simulations, the total power budget p is set to 1 in different scenarios, while the noise variance varies depending on the SNR. To ensure a fair comparison, we first obtain the optimal solution and the closed-form solution to the conventional linear SB-BLP problem and the RZF precoding, and then rescale these solutions to meet the symbol-level power constraint.

Fig. 4 depicts the BER performance versus the increasing SNR for the aforementioned two fully-loaded MU-MISO configurations. The stopping criterion is set to $\Delta < 1\times 10^{-3}$, where $\Delta \triangleq \left\|\mathbf{x}^t - \mathbf{x}^{t-1}\right\|$ denotes the iteration decrease,

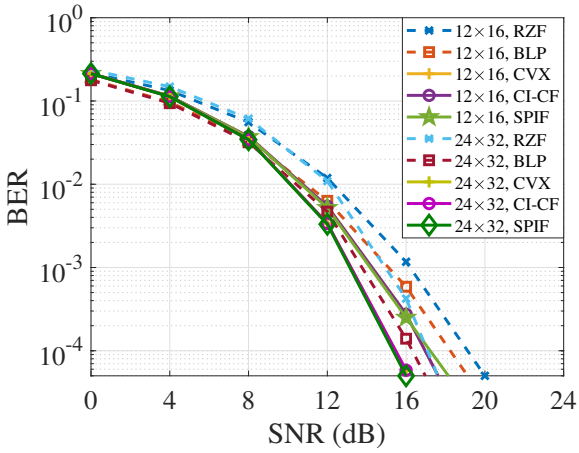

Fig. 5. BER versus SNR for two under-loaded MU-MISO configurations, $T = 40$, $N_c = 500$, $N_s = 20$, QPSK.

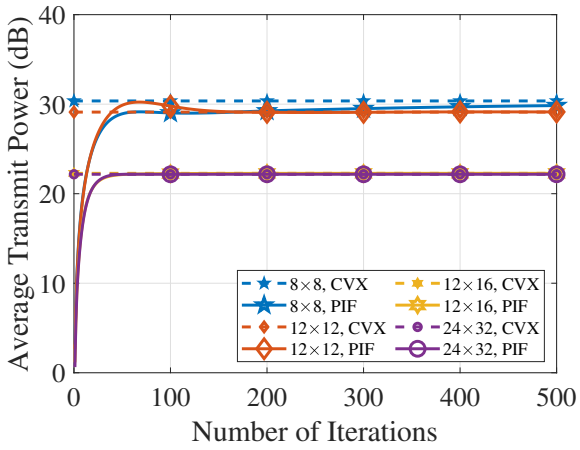

Fig. 6. Average transmit power versus number of iterations for various MU-MISO configurations, $Nc = 100$, $N_s = 20$, 16QAM.

and the maximum number of iterations $T_{max} = 100$. The fully-loaded system may have strong interfering channels that require a more accurate transmit signal than the under-loaded system in order to exploit interference. This criterion ensures an acceptable level of accuracy while maintaining a reasonable iteration scale. We can observe in Fig. 4 that the BER performance of the proposed SPIF-SLP algorithm is well approximated to that of the CVX and CI-CF in fully-loaded systems with PSK signaling.

As for the aforementioned two under-loaded MU-MISO configurations, Fig. 5 illustrates their BER performance as a function of the increasing SNR. It can be observed that the BER performance of the proposed SPIF-SLP algorithm is almost consistent with that of the selected benchmark SB-SLP algorithms. This observation validates the effectiveness of the proposed SPIF-SLP algorithm for PSK modulation in under-loaded scenarios.

TABLE I
AVERAGE EXECUTION TIME PER FRAME IN SEC. FOR SB-SLP, SNR $= 24$ DB AND $N_c = 100$ FOR FULLY-LOADED SYSTEMS, SNR $= 16$ DB AND $N_c = 500$ FOR UNDER-LOADED SYSTEMS, $N_s = 20$, QPSK.

	8×8	12×12	12×16	24×32
RZF	7.7550e-5	9.9942e-5	1.3305e-4	3.8623e-4
BLP	6.3492e-3	8.8139e-3	1.1864e-2	5.1872e-2
CVX	5.1499	5.0931	5.2272	5.4476
CI-CF	6.9108e-3	8.7573e-3	7.9728e-3	2.9464e-2
SPIF	**2.0446e-3**	**3.1874e-3**	**1.6692e-3**	**6.4658e-3**

Table I lists the time complexity, in terms of the average execution time per frame, of the compared algorithms for the SB-SLP problem with PSK modulation under four MU-MISO configurations. The number of iterations of the SPIF-SLP algorithm is the same as that in Fig. 4 and Fig. 5. The execution time of the proposed SPIF-SLP algorithm for PSK modulation is approximately 29.6%, 36.4%, 5.2%, and 20.9% of that of the CI-CF algorithm in 8×8, 12×12, 12×16, and 24×32 MU-MISO configurations, respectively. The complexity reduction of the proposed SPIF-SLP algorithm for PSK modulation is appealing in all the considered MU-MISO configurations.

Next, the average transmit power and the time complexity of the proposed PIF-SLP algorithm for QAM modulation are investigated in terms of the average execution time per frame. Consider the unit noise variance, $\sigma_k^2 = \sigma^2 = 1$, along with an equal instantaneous SINR threshold for each user, i.e., $\gamma_k = \gamma, \forall k$.

Again, to demonstrate the convergence of the proposed PIF-SLP algorithm for QAM modulation, we present the average transmit power versus the number of iterations for four MU-MISO configurations in Fig. 6. The results are averaged over $N_c = 100$ random channel realizations. The SINR threshold is set to 18 dB, and the penalty parameter is set to 0.8 for both 8×8 and 12×12 MU-MISO configurations. Regarding the two under-loaded MU-MISO configurations, it is evident that the PIF-SLP algorithm requires approximately 150 iterations to approach the benchmark scheme. However, the two challenging fully-loaded MU-MISO configurations may necessitate hundreds or thousands of iterations to achieve convergence. Compared to the previous PSK case, the proposed PIF-SLP algorithm for QAM modulation needs more iterations to converge because the correct detection of QAM modulation relies on both the amplitude and phase of the received signal, thus requiring a more accurate transmit signal.

Fig. 7 illustrates the average transmit power performance of the proposed PIF-SLP algorithm for QAM modulation as a function of the SINR threshold for two fully-loaded MU-MISO configurations. The penalty parameter is set to 0.8. It shows that the performance of the proposed PIF-SLP algorithm is well-matched with the benchmark SLP schemes. The BER gap between the conventional linear BLP and SLP is prominent in these fully-loaded cases, where there is more interference to be exploited.

Fig. 8 shows the average transmit power performance of the proposed PIF-SLP algorithm for QAM modulation as a function of the SINR threshold for two under-loaded MU-MISO configurations. The performance of the proposed PIF-SLP algorithm matches that of the CVX and the EGPA at

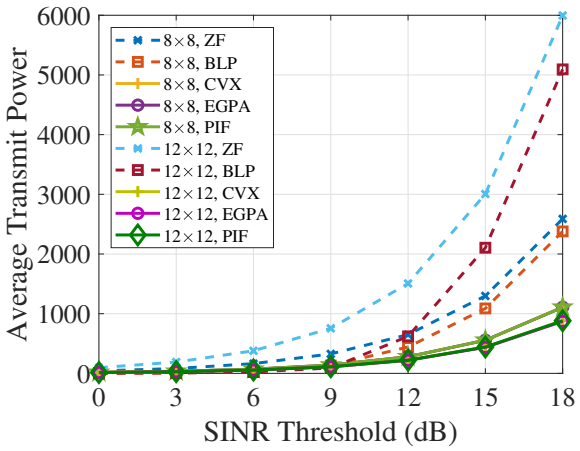

Fig. 7. Average transmit power versus SINR threshold for two fully-loaded MU-MISO configurations, $\Delta < 1 \times 10^{-7}$ for 8×8, $\Delta < 1 \times 10^{-6}$ for 12×12, $T_{max} = 4000$, $N_c = 100$, $N_s = 20$, 16QAM.

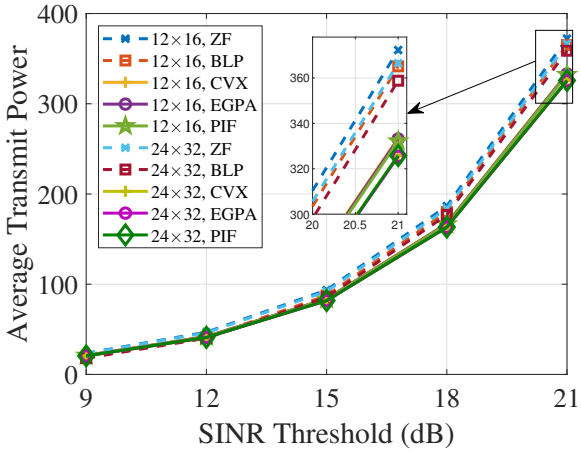

Fig. 8. Average transmit power versus SINR threshold for two under-loaded MU-MISO configurations, $T = 150$, $Nc = 100$, $N_s = 20$, 16QAM.

various MU-MISO configurations and SINR thresholds. These results imply that the proposed PIF-SLP algorithm guarantees optimality for QAM modulation after adequate iterations. The average transmit power of the PM-SLP problem is significantly impacted by the system load. Interestingly, despite having different numbers of transmit and receive antennas, the two MU-MISO configurations consume almost equal transmit power while serving different numbers of users due to the same system load level.

TABLE II
AVERAGE EXECUTION TIME IN SEC. FOR PM-SLP, $\gamma = 18$ DB, $N_c = 100$, $Ns = 20$, 16QAM.

	8×8	12×12	12×16	24×32
ZF	7.8163e-5	9.3746e-5	1.0928e-4	3.8348e-4
BLP	1.6017e-2	2.5975e-2	3.8003e-2	1.8405e-1
CVX	3.7960	3.4524	3.4575	3.5514
EGPA	2.6707	3.4661	4.3924e-1	2.5850
PIF	**4.4405e-2**	**5.5317e-2**	**7.6179e-3**	**1.3476e-2**

Table II further compares the average execution time per

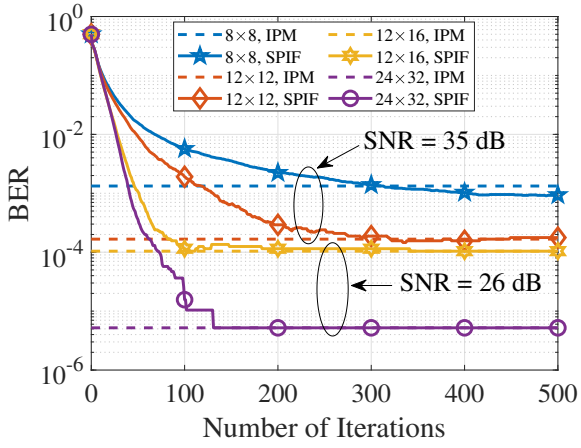

Fig. 9. BER versus number of iterations, $N_c = 100$, $N_s = 20$, 16QAM.

frame of the considered algorithms for the PM-SLP problem with QAM modulation, where the parameters are the same as those in Fig. 7 and Fig. 8. Due to its simple and inverse-free processing, the proposed PIF-SLP algorithm exhibits the fastest speed in solving the PM-SLP problem with QAM modulation, compared to the CVX and the EGPA. Specifically, in 8×8, 12×12, 12×16, and 24×32 MU-MISO configurations, the proposed PIF-SLP algorithm provides processing times that are 60.14, 62.66, 57.66, and 191.82 times faster than the EGPA, respectively. It can also provide a processing time that is 85.49, 62.41, 453.89, and 263.54 times faster than the CVX in 8×8, 12×12, 12×16, and 24×32 MU-MISO configurations, respectively. Note that the execution time of the PIF-SLP algorithm can be significantly reduced by implementing it in parallel, making it more efficient in practice.

Similar to the PSK case, the SPIF-SLP algorithm for QAM modulation involves evaluating the necessary number of iterations for convergence. This evaluation is performed in Fig. 9, where the BER is shown as a function of the number of iterations. The results are an average of 2000 symbol slots. The benchmark scheme is the IPM implemented by the CVX software package [38]. We set SNR $=$ 26 dB and SNR $=$ 35 dB for under-loaded and fully-loaded MU-MISO configurations, respectively. After 150 iterations, the BER of the SPIF-SLP algorithm for two under-loaded MU-MISO configurations can converge to that of the CVX. Consequently, we set the number of iterations of the SPIF-SLP algorithm to 150 for the remaining under-loaded simulations. In contrast, the fully-loaded MU-MISO configurations require significantly more iterations to achieve convergence.

Fig. 10 depicts the BER performance of the proposed SPIF-SLP algorithm for QAM modulation versus the increasing SNR for two fully-loaded MU-MISO configurations. It can be observed that the SPIF algorithm can approach the performance of the CVX in fully-loaded systems with QAM signaling. Additionally, the enhanced superiority of SLP over BLP can also be observed in the fully-loaded systems.

Fig. 11 depicts the BER performance of the proposed SPIF-SLP algorithm for QAM modulation versus the increasing SNR for the aforementioned two under-loaded MU-MISO

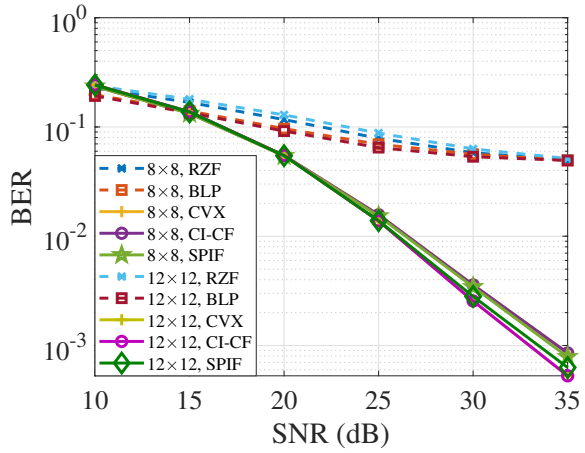

Fig. 10. BER versus SNR for two fully-loaded MU-MISO configurations, $\Delta < 1 \times 10^{-4}$, $T_{max} = 250$ for 8×8, $T_{max} = 300$ for 12×12, $N_c = 500$, $N_s = 20$, 16QAM.

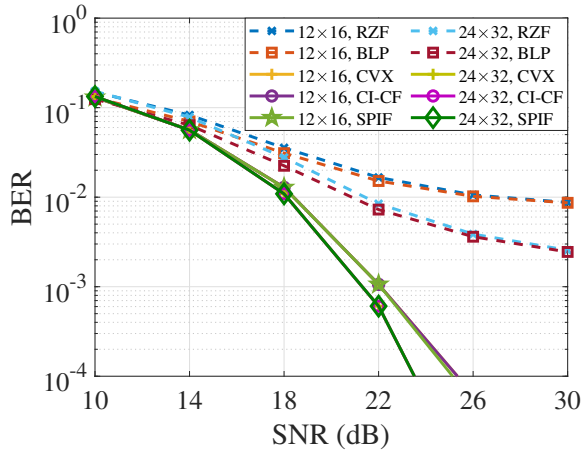

Fig. 11. BER versus SNR for two under-loaded MU-MISO configurations, $T = 150$, $N_c = 200$, $N_s = 20$, 16QAM.

configurations. The benchmark schemes are selected as the same as the PSK case. The same trends can be seen in Fig. 11 and Fig. 5. The BER performance of the proposed SPIF-SLP algorithm is almost consistent with that of the selected benchmark SLP algorithms. This validates the effectiveness of the proposed SPIF-SLP algorithm for QAM modulation.

TABLE III
AVERAGE EXECUTION TIME PER FRAME IN SEC. FOR SB-SLP, SNR $= 35$ DB AND $N_c = 500$ FOR FULLY-LOADED SYSTEMS, SNR $= 26$ DB AND $N_c = 200$ FOR UNDER-LOADED SYSTEMS, $N_s = 20$, 16QAM.

	8×8	12×12	12×16	24×32
RZF	8.4053e-5	1.0466e-4	1.3507e-4	4.5374e-4
BLP	4.3733e-2	4.4343e-2	6.3672e-2	3.0584e-1
CVX	5.0293	5.0515	5.2681	5.9227
CI-CF	1.1869e-2	1.8267e-2	1.8267e-2	8.3196e-2
SPIF	**1.2957e-2**	**1.6893e-2**	**8.8743e-3**	**1.5851e-2**

Table III lists the time complexity in terms of the average execution time per frame of the compared algorithms for the SB-SLP problem with QAM modulation under four MU-MISO configurations, where the parameters are the same as those in Fig. 10 and Fig. 11. The execution time of the proposed SPIF-SLP algorithm for QAM modulation is about 109.2%, 92.5%, 48.6%, and 19.1% of that of the CI-CF algorithm in 8×8, 12×12, 12×16, and 24×32 MU-MISO configurations, respectively. The complexity reduction of the proposed SPIF-SLP algorithm is prominent for QAM modulation in the under-loaded MU-MISO configurations. For 8×8 and 12×12 MU-MISO configurations, the comparable execution time of the SPIF and CI-CF can be observed in Table III. On the one hand, in the fully-loaded systems with QAM signaling, the CI-CF takes fewer iterations to converge due to the smaller search space, i.e., fewer constellation points can exploit interference compared to the PSK case. On the other hand, for the SPIF-SLP algorithm, the number of iterations of the SPIF-SLP algorithm is boosted by both the symmetric channel and QAM signaling. This can be alleviated by parallel implementation in practice.

VII. CONCLUSION

In this work, we have presented an explicit duality between two typical SLP problems, i.e., the PM-SLP problem as well as the weighted max-min SB-SLP problem, and proposed low-complexity SLP algorithms for both PSK and QAM modulations. The proposed duality analytically shows underlying connections between the two distinct types of problems in closed form. Moreover, a one-step power scaling algorithm has been developed to solve the inseparable SB-SLP problem on prior knowledge of the corresponding PM-SLP solution. Furthermore, the revealed separability of the PM-SLP problem with QAM modulation induces the modified PIF-SLP algorithm, which decomposes the problem into multiple parallel subproblems with simple closed-form solutions. The duality has been further extended to QAM modulation. Jointly considering the power scaling algorithm and the modified PIF-SLP algorithm, we have developed a SPIF-SLP algorithm for the SB-SLP problem. Through numerical results, both the modified PIF-SLP and SPIF-SLP algorithms have been shown to provide low-complexity features while guaranteeing optimal performance.

The duality, separability analysis, and decomposition methodology in this paper are general for a variety of SLP designs. Future work based on this paper would be efficient algorithm designs for robust SLP under CSI uncertainty and/or quantized CSI. Other promising research can be low-complexity ADMM solutions for CI-BLP, as the extension to CI-BLP is significant but not trivial.

REFERENCES

[1] J. Yang, A. Li, X. Liao, and C. Masouros, "Duality between the power minimization and max-min SINR balancing symbol-level precoding," in *Proc. IEEE 97th Veh. Technol. Conf. (VTC2023-Spring)*, Florence, Italy, Jun. 2023, pp. 1–6.

[2] I.-H. Wang and D. N. C. Tse, "Interference mitigation through limited receiver cooperation," *IEEE Trans. Inf. Theory*, vol. 57, no. 5, pp. 2913–2940, May 2011.

[3] C. Windpassinger, R. Fischer, T. Vencel, and J. Huber, "Precoding in multiantenna and multiuser communications," *IEEE Trans. Wireless Commun.*, vol. 3, no. 4, pp. 1305–1316, Jul. 2004.

[4] M. Costa, "Writing on dirty paper (corresp.)," *IEEE Trans. Inf. Theory*, vol. 29, no. 3, pp. 439–441, May 1983.

[5] M. Tomlinson, "New automatic equaliser employing modulo arithmetic," *Electron. Lett.*, vol. 7, no. 5, pp. 138–139, Mar. 1971.

[6] H. Harashima and H. Miyakawa, "Matched-transmission technique for channels with intersymbol interference," *IEEE Trans. Commun.*, vol. 20, no. 4, pp. 774–780, Aug. 1972.

[7] B. Hochwald, C. Peel, and A. Swindlehurst, "A vector-perturbation technique for near-capacity multiantenna multiuser communication-part II: perturbation," *IEEE Trans. Commun.*, vol. 53, no. 3, pp. 537–544, Jan. 2005.

[8] G. Caire and S. Shamai, "On the achievable throughput of a multiantenna gaussian broadcast channel," *IEEE Trans. Inf. Theory*, vol. 49, no. 7, pp. 1691–1706, Jul. 2003.

[9] C. Peel, B. Hochwald, and A. Swindlehurst, "A vector-perturbation technique for near-capacity multiantenna multiuser communication-part I: channel inversion and regularization," *IEEE Trans. Commun.*, vol. 53, no. 1, pp. 195–202, Jan. 2005.

[10] E. Visotsky and U. Madhow, "Optimum beamforming using transmit antenna arrays," in *Proc. IEEE 49th Veh. Technol. Conf.*, Houston, TX, USA, May 1999, pp. 851–856.

[11] D. Palomar, J. Cioffi, and M. Lagunas, "Joint Tx-Rx beamforming design for multicarrier MIMO channels: a unified framework for convex optimization," *IEEE Trans. Signal Process.*, vol. 51, no. 9, pp. 2381–2401, Sep. 2003.

[12] M. Schubert and H. Boche, "Solution of the multiuser downlink beamforming problem with individual SINR constraints," *IEEE Trans. Veh. Technol.*, vol. 53, no. 1, pp. 18–28, Jan. 2004.

[13] A. Wiesel, Y. Eldar, and S. Shamai, "Linear precoding via conic optimization for fixed MIMO receivers," *IEEE Trans. Signal Process.*, vol. 54, no. 1, pp. 161–176, Jan. 2006.

[14] S. S. Christensen, R. Agarwal, E. De Carvalho, and J. M. Cioffi, "Weighted sum-rate maximization using weighted MMSE for MIMO-BC beamforming design," *IEEE Trans. Wireless Commun.*, vol. 7, no. 12, pp. 4792–4799, Dec. 2008.

[15] C. Masouros and G. Zheng, "Exploiting known interference as green signal power for downlink beamforming optimization," *IEEE Trans. Signal Process.*, vol. 63, no. 14, pp. 3628–3640, Jul. 2015.

[16] M. Alodeh, S. Chatzinotas, and B. Ottersten, "Constructive multiuser interference in symbol level precoding for the MISO downlink channel," *IEEE Trans. Signal Process.*, vol. 63, no. 9, pp. 2239–2252, May 2015.

[17] A. Li, D. Spano, J. Krivochiza, S. Domouchtsidis, C. G. Tsinos, C. Masouros, S. Chatzinotas, Y. Li, B. Vucetic, and B. Ottersten, "A tutorial on interference exploitation via symbol-level precoding: Overview, state-of-the-art and future directions," *IEEE Commun. Surv. Tut.*, vol. 22, no. 2, pp. 796–839, Secondquarter 2020.

[18] M. Alodeh, D. Spano, A. Kalantari, C. G. Tsinos, D. Christopoulos, S. Chatzinotas, and B. Ottersten, "Symbol-level and multicast precoding for multiuser multiantenna downlink: A state-of-the-art, classification, and challenges," *IEEE Commun. Surv. Tut.*, vol. 20, no. 3, pp. 1733–1757, Thirdquarter 2018.

[19] H. Jedda, A. Mezghani, J. A. Nossek, and A. L. Swindlehurst, "Massive MIMO downlink 1-bit precoding with linear programming for PSK signaling," in *Proc. IEEE 18th Int. Workshop Signal Process. Adv. Wireless Commun. (SPAWC)*, Sapporo, Japan, Jul. 2017, pp. 1–5.

[20] F. Askerbeyli, W. Xu, and J. A. Nossek, "1-bit precoding for massive MIMO downlink with linear programming and a greedy algorithm extension," in *Proc. IEEE 93rd Veh. Technol. Conf. (VTC2021-Spring)*, Helsinki, Finland, Apr. 2021, pp. 1–5.

[21] C. Masouros and E. Alsusa, "A novel transmitter-based selective-precoding technique for DS/CDMA systems," *IEEE Signal Process. Lett.*, vol. 14, no. 9, pp. 637–640, Sep. 2007.

[22] C. Masouros, "Correlation rotation linear precoding for MIMO broadcast communications," *IEEE Trans. Signal Process.*, vol. 59, no. 1, pp. 252–262, Jan. 2011.

[23] C. Masouros, T. Ratnarajah, M. Sellathurai, C. B. Papadias, and A. K. Shukla, "Known interference in the cellular downlink: a performance limiting factor or a source of green signal power?" *IEEE Commun. Mag.*, vol. 51, no. 10, pp. 162–171, Oct. 2013.

[24] M. Alodeh, S. Chatzinotas, and B. Ottersten, "Symbol-level multiuser MISO precoding for multi-level adaptive modulation," *IEEE Trans. Wireless Commun.*, vol. 16, no. 8, pp. 5511–5524, Aug. 2017.

[25] A. Haqiqatnejad, F. Kayhan, and B. Ottersten, "Symbol-level precoding design based on distance preserving constructive interference regions," *IEEE Trans. Signal Process.*, vol. 66, no. 22, pp. 5817–5832, Nov. 2018.

[26] ——, "Power minimizer symbol-level precoding: A closed-form suboptimal solution," *IEEE Signal Process. Lett.*, vol. 25, no. 11, pp. 1730–1734, Nov. 2018.

[27] ——, "An approximate solution for symbol-level multiuser precoding using support recovery," in *Proc. IEEE Int. Workshop Signal Process. Adv. Wireless Commun. (SPAWC)*, Cannes, France, Jul. 2019, pp. 1–5.

[28] A. Li and C. Masouros, "Interference exploitation precoding made practical: Optimal closed-form solutions for PSK modulations," *IEEE Trans. Wireless Commun.*, vol. 17, no. 11, pp. 7661–7676, Nov. 2018.

[29] A. Li, C. Masouros, B. Vucetic, Y. Li, and A. L. Swindlehurst, "Interference exploitation precoding for multi-level modulations: Closed-form solutions," *IEEE Trans. Commun.*, vol. 69, no. 1, pp. 291–308, Jan. 2021.

[30] A. Li, C. Shen, X. Liao, C. Masouros, and A. L. Swindlehurst, "Practical interference exploitation precoding without symbol-by-symbol optimization: A block-level approach," *IEEE Trans. Wireless Commun.*, vol. 22, no. 6, pp. 3982–3996, Jun. 2023.

[31] Z. Xiao, R. Liu, M. Li, Y. Liu, and Q. Liu, "Low-complexity designs of symbol-level precoding for MU-MISO systems," *IEEE Trans. Commun.*, vol. 70, no. 7, pp. 4624–4639, Jul. 2022.

[32] J. Yang, A. Li, X. Liao, and C. Masouros, "Low complexity SLP: An inversion-free, parallelizable ADMM approach," *arXiv preprint arXiv:2209.12369*, Sep. 2022. [Online]. Available: https://arxiv.org/abs/2209.12369

[33] A. Haqiqatnejad, F. Kayhan, and B. Ottersten, "Constructive interference for generic constellations," *IEEE Signal Process. Lett.*, vol. 25, no. 4, pp. 586–590, Apr. 2018.

[34] E. Karipidis, N. D. Sidiropoulos, and Z.-Q. Luo, "Quality of service and max-min fair transmit beamforming to multiple cochannel multicast groups," *IEEE Trans. Signal Process.*, vol. 56, no. 3, pp. 1268–1279, Mar. 2008.

[35] M. Sadeghi, L. Sanguinetti, R. Couillet, and C. Yuen, "Reducing the computational complexity of multicasting in large-scale antenna systems," *IEEE Trans. Wireless Commun.*, vol. 16, no. 5, pp. 2963–2975, May 2017.

[36] K. L. Law and C. Masouros, "Symbol error rate minimization precoding for interference exploitation," *IEEE Trans. Commun.*, vol. 66, no. 11, pp. 5718–5731, Nov. 2018.

[37] W. Deng, M.-J. Lai, Z. Peng, and W. Yin, "Parallel multi-block ADMM with o (1/k) convergence," *J. Sci. Comput.*, vol. 71, no. 2, pp. 712–736, May 2017.

[38] M. Grant and S. Boyd, *CVX: MATLAB software for disciplined convex programming, version 2.1*, Mar. 2014. [Online]. Available: http://cvxr.com/cvx

Junwen Yang (S'23) received the B.S. degree in electronic information engineering and the M.S. degree in electronic and communication engineering from Central China Normal University, Wuhan, China, in 2017 and 2019, respectively. He is working toward the Ph.D. degree with the School of Information and Communications Engineering, Xi'an Jiaotong University, Xi'an, China. His current research interests mainly focus on wireless communications, signal processing, optimizations, and symbol-level precoding.

Ang Li (S'14-M'18-SM'21) received his Ph.D. degree in the Communications and Information Systems research group, Department of Electrical and Electronic Engineering, University College London in April 2018. He was a postdoctoral research associate in the School of Electrical and Information Engineering, The University of Sydney from May 2018 to February 2020. He joined Xi'an Jiaotong University in March 2020 and is now a Professor in the School of Information and Communications Engineering, Faculty of Electronic and Information Engineering, Xi'an Jiaotong University, Xi'an, China. His main research interests lie in the physical-layer techniques in wireless communications, including MIMO/massive MIMO, interference exploitation, symbol-level precoding, and reconfigurable MIMO, etc. He currently serves as the Associate Editor for IEEE COMMUNICATIONS LETTERS, IEEE OPEN JOURNAL OF SIGNAL PROCESSING, and EURASIP JOURNAL ON WIRELESS COMMUNICATIONS AND NETWORKING. He is the recipient of the 2021 IEEE Signal Processing Society Young Author Best Paper Award. He has been an Exemplary Reviewer for IEEE COMMUNICATIONS LETTERS, IEEE TRANSACTIONS ON COMMUNICATIONS, and IEEE WIRELESS COMMUNICATIONS LETTERS. He has served as the Co-Chair of the IEEE ICASSP 2020 Special Session on 'Hardware-Efficient Large-Scale Antenna Arrays: The Stage for Symbol-Level Precoding', and has organized a Tutorial in IEEE ICC 2021 on 'Interference Exploitation through Symbol Level Precoding: Energy Efficient Transmission for 6G and Beyond'.

Xuewen Liao received the B.S. and Ph.D. degrees in information and communications engineering from Xi'an Jiaotong University, Xi'an, China, in 2002 and 2008, respectively. From 2008 to 2012, he was an Assistant Professor at Xi'an Jiaotong University. From 2016 to 2017, he was a Visiting Scholar at the Department of Electrical and Computer Engineering, The University of British Columbia, Vancouver, BC, Canada. He is currently an Associate Professor with the School of Information and Communications Engineering, Xi'an Jiaotong University. His research interests include wireless energy transfer, green communications, relay communications, and indoor positioning.

Christos Masouros (Senior Member, IEEE) received the Diploma degree in Electrical and Computer Engineering from the University of Patras, Greece, in 2004, and MSc by research and PhD in Electrical and Electronic Engineering from the University of Manchester, UK in 2006 and 2009 respectively. In 2008 he was a research intern at Philips Research Labs, UK, working on the LTE standards. Between 2009-2010 he was a Research Associate in the University of Manchester and between 2010-2012 a Research Fellow in Queen's University Belfast. In 2012 he joined University College London as a Lecturer. He has held a Royal Academy of Engineering Research Fellowship between 2011-2016.

Since 2019 he is a Full Professor of Signal Processing and Wireless Communications in the Information and Communication Engineering research group, Dept. Electrical and Electronic Engineering, and affiliated with the Institute for Communications and Connected Systems, University College London. His research interests lie in the field of wireless communications and signal processing with particular focus on Green Communications, Large Scale Antenna Systems, Integrated Sensing and Communications, interference mitigation techniques for MIMO and multicarrier communications. Between 2018-22 he was the Project Coordinator of the €4.2m EU H2020 ITN project PAINLESS, involving 12 EU partner universities and industries, towards energy-autonomous networks. Between 2024-28 he will be the Scientific Coordinator of the €2.7m EU H2020 DN project ISLANDS, involving 19 EU partner universities and industries, towards next generation vehicular networks. He was the recipient of the 2023 IEEE ComSoc Stephen O. Rice Prize, co-recipient of the 2021 IEEE SPS Young Author Best Paper Award and the recipient of the Best Paper Awards in the IEEE GlobeCom 2015 and IEEE WCNC 2019 conferences. He has been recognised as an Exemplary Editor for the IEEE COMMUNICATIONS LETTERS, and as an Exemplary Reviewer for the IEEE TRANSACTIONS ON COMMUNICATIONS. He is an Editor for IEEE TRANSACTIONS ON WIRELESS COMMUNICATIONS, the IEEE OPEN JOURNAL OF SIGNAL PROCESSING, and Editor-at-Large for IEEE OPEN JOURNAL OF THE COMMUNICATIONS SOCIETY. He has been an Editor for IEEE TRANSACTIONS ON COMMUNICATIONS, IEEE COMMUNICATIONS LETTERS, and a Guest Editor for a number of IEEE JOURNAL ON SELECTED TOPICS IN SIGNAL PROCESSING and IEEE JOURNAL ON SELECTED AREAS IN COMMUNICATIONS issues. He is a founding member and Vice-Chair of the IEEE Emerging Technology Initiative on Integrated Sensing and Communications (SAC), Vice Chair of the IEEE Wireless Communications Technical Committee Special Interest Group on ISAC, and Chair of the IEEE Green Communications & Computing Technical Committee, Special Interest Group on Green ISAC. He is the TPC chair for the IEEE ICC 2024 Selected Areas in Communications (SAC) Track on ISAC.